Imperial College London

Assessment of Fidelity in the Presence of Initialization and Measurement Errors in Noisy Intermediate-Scale Quantum devices

Maria Isabel Franco Garrido

A dissertation submitted in partial fulfillment of
the requirements for the degree of

MSc in Quantum Fields and Fundamental Forces

at
Imperial College London

supervised by
Professor Florian Mintert

October, 2021

Abstract

Improvements in the implementations of quantum circuits in noisy devices are one of the main challenges to target in order to benefit from the currently available quantum computers – the NISQ devices. The recent accurate implementations of quantum gates have opened a search of other possible sources of noise that could be affecting the quantum circuits.

This thesis works in assessing how errors in the initialization and measurement affect the quality of the dynamics of a quantum circuit. We use Quantum Process Tomography and gate fidelity to discover this impact through the application of different types of errors. In particular, we study the impact of incoherent classical noise, encoded as CPTP maps, to the reconstruction of Pauli gates. Our method is first established for Pauli gates for a 1-qubit system and then extended to a 2-qubit system. In both cases we find that the influence of these errors on fidelity is considerably small. An expansion to 3-qubits and beyond is possible but computationally challenging. We will also establish the theoretical baseline to confront some of the limitations for possible future work.

Acknowledgements

I would like to express my sincere gratitude to my thesis supervisor, Professor Florian Mintert, for the consistent support and guidance offered throughout the summer.

Contents

List of Figures

Chapter 1

Introduction

1.1 Research Motivation

Quantum Computation is a continuously growing field with an enormous potential to revolutionize different areas, ranging from science to industry. It is currently reaching what John Preskill named the "Noise intermediate scale quantum (NISQ) devices era" [3], where we have available computers with enough qubits to surpass a classical computer but not enough to reach Quantum Supremacy. We label these "Noisy" due to their imperfect performance and "intermediate" due to their limited qubit availability.

Increasing the number of qubits in these computers would allow them to reach their full potential. Nevertheless, we can still expect a few hundreds of qubits to be enough to solve computationally challenging problems in a classical setting. It is therefore interesting to develop further the NISQ devices.

In order to improve them, we must think of ways to mitigate the noise. The main source of issues comes from current technology hindering the full cohesion between Quantum software and Quantum Hardware [4]. There are several approaches to tackle this. Quantum Error Correction (QEC) is the most direct strategy, but unfortunately, it requires a very large increase in the number of qubits, which is currently not possible. It is consequently essential that we look into error mitigation [5]. This technique is based on combining additional measurement data with classical post-processing such that relatively noise-free results can be extracted from noisy devices.

For NISQ devices, Quantum Error mitigation is thus the fundamental tool for improvement. However, we must grow an extensive knowledge in

Quantum Errors to further develop these into fault-tolerant quantum computers through error mitigation. We can find quantum computers errors in the preparation, channel and measurement phases.

Recently, there have been significant improvements in the implementations of the quantum gates [6], but we still experience faulty operations. The presence of this noisiness takes us to revise other possible places of errors. Hence, it is imperative to provide a further study on the initialization and measurement errors in order to check the source of this noisiness.

1.2 Research Objectives

Our primary goal is to estimate the error level at which different initialization and measurement mistakes affect our quantum systems. From a higher standpoint, we hope this can translate to a better understanding of Quantum Errors and contribute to guide the efforts in the research for QEM.

We want to provide tangible results on the effect of different types of possible errors on gate fidelity. The **main hypothesis** of this research states that:

"We analyse the effect of different errors in the input states and measurement through gate reconstruction, to provide an insight and improve our understanding in the errors of quantum circuits running on NISQ devices."

To achieve this hypothesis, the **main task** for this project is to:

Investigate the correlation between input and measurement errors and the quality of the dynamics of a quantum system via gate reconstruction and gate fidelity.

1.3 Project Approach

Our approach to demonstrating the relationship between the input and measurement errors and the noisiness in the quantum circuits is divided into multiple steps:

- The first step consists in studying and reviewing Quantum Noise and the state-of-the-art techniques in Quantum Error Correction and Quantum Error Mitigation to put our thesis in context.

- Secondly, we analyse the Quantum Tomography techniques to find the appropriate gate reconstruction procedure. We pick Standard Quantum Process Tomography which is suitable for the errors and gates we wish to study, and therefore serves our purpose.

- We then move to study appropriate methods to model errors. To do this, we review the ways in which we can encode them, and in order to apply our gate reconstruction model, we select a specific type of errors – incoherent errors. This choice is motivated by the latest discoveries in the research in this area.

- We compute the results for the gate fidelity of different Pauli gates and the aforementioned errors and provide a graphical illustration of those.

It is worth mentioning that we build and analyse the methodology above for 1 and 2 qubits by translating the theoretical work to a Mathematica code base in order to perform the corresponding operations. We also reflect on other possible state-of-the-art methods to apply for the possible expansion of our work to 3 qubits and to a more experimental-friendly setting.

1.4 Scientific Contributions

The major contribution of this research is a robust proof of the claim that fidelity is not greatly impacted by the appearance of the selected input and/or measurement errors. It is therefore possible to perform considerable quantum circuits even in the presence of these errors. Consequently, the noise in the quantum systems could potentially come either from different error sources or from other unchecked parts of the quantum circuit, like ancilla qubits.

Even more, we designed an algorithm that performs Quantum Processs Tomography under the presence of errors produced by CPTP maps and which calculates the gate fidelity of the process. Using this model could prove to

be very useful for researchers who are trying to get an idea of whether or not a certain error might impact their quantum circuit. For instance, the researcher can look to measure the error impact theoretically with this tool. This can be specially useful to perform a general check of performance with no further use of more qubits or assessment on the qubit directly, and serve as a help to the study of Quantum Error Mitigation.

An interesting facet of our thesis is the robustness of the obtained results. Indeed, we conduct in most of the cases a reconstruction and a fidelity estimation with a heavily randomised application of the errors. The objective of this is to proof our method against a real physical noise so that our results are closer to an experimental setting.

Additionally, to the best of our knowledge, this thesis is the first to insert different initialization and measurement incoherent errors in SQPT to predict their effect on quantum circuit dynamics. Exploiting the possible applications of QPT is a very interesting task and it is an honour to be able to make good use of it. Finally, with our comments on a further expansion of this model we hope to motivate a continuation of this research.

Chapter 2

Literature Review

2.1 NISQ Devices

This section reviews the concept of NISQ devices, their current availability, capabilities, and issues. We also want to highlight their importance in the final composition of a quantum computer that reaches quantum supremacy and hence the relevance of working towards its improvements.

Quantum annealers, Noise Intermediate-Scale Quantum computers and fault-tolerant universal quantum computers are the three categories in which we can classify quantum computers. Quantum annealing [7] involves controlling fluctuations in quantum states to perform calculations instead of sending them through gates in a circuit. The most popular available quantum annealers are from D-Wave, which has announced a 5000-qubit quantum computer. However, quantum annealers are not on the development path that leads to fault-tolerant universal quantum machines. Therefore, NISQ sets itself as the only candidate towards the ultimate goal of quantum supremacy by building fault-tolerant universal quantum computer.

Currently, the most exploited systems of qubits are photons, trapped ions, superconducting circuits and spins in semiconductors. Major breakthroughs have been recently made such as constructing a quantum computer with above 50 superconducting qubits [8], or trapped ions [9]. Trapped and detected cold atoms produced two hundred fifty-six qubits in optical tweezers (arrays of ultra-cold atoms) [10]. About 76 light-based qubits have been reached [11]. Although, currently, only devices between 5-79 qubits are available to the general public.

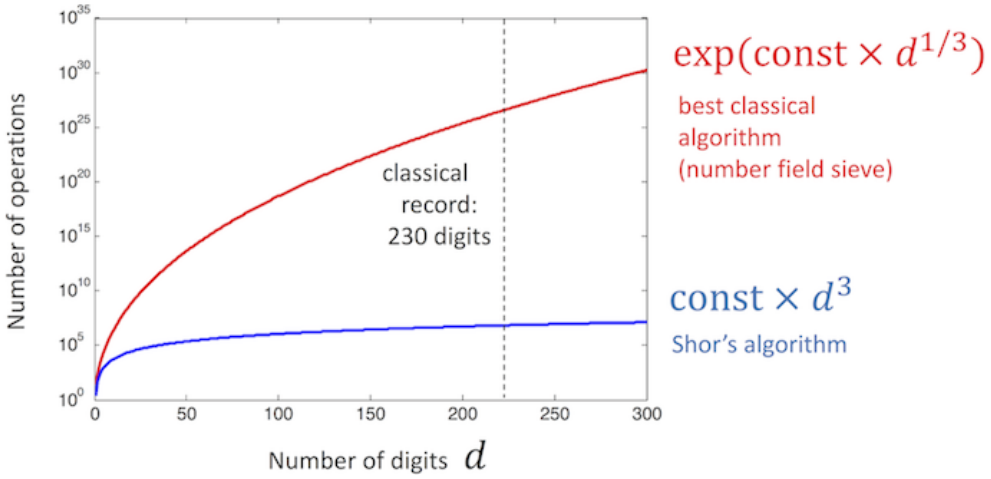

Figure 2.1: Comparison between the number of operations used by Shor's and the General number field sieve algorithm to factorise a number with d number of digits [1].

Historically, one of the most famous algorithms which served as a proof of quantum advantage was Shor's algorithm [12] for factoring integers, which became famous for being a threat to the current security systems. This algorithm is an evidence that NISQ can be superior to classical computers in certain tasks.

If N is the number to be factorized, and $d \sim \log_2(N)$ is the number of digits, Shor's algorithm has complexity $O(d^3)$. Whereas, the General number field sieve algorithm [13] has an exponential asymptotic run-time to the number of digits, it has complexity of $O(e^{d^{\frac{1}{3}}})$

As we can see in Figure 2.1, for the case of qubits between 10-100, we can already notice a clear reduction on the number of operations and hence on the computational time when we use the quantum computer versus the classical.

Looking at the figure 2.1, we can see that we require many qubits far beyond 300 to perform the factorization that threatens our current systems.

We must remain patient since quantum computers will not reach the so-called quantum supremacy until more qubits are in place [14]. Nevertheless, it is also true that their full potential remains unexplored. The power of NISQ devices is becoming more evident. Recent examples include a sampling task quantum algorithm finished by Zuchongzhi Quantum Computer

in about 1.2 hours which would take the most powerful supercomputer at least eight years [15]. Sampling algorithms are used in statistical models, and they are procedures that extract a suitable unit from a population. This advance represents a giant leap for fields such as machine learning or data science. We have also seen other exponential speedups against their classical counterpart e.g. Recommendations systems [16]

Therefore, as we can see, it is in our best interest to advance on developing NISQ devices in order to be as close to fault-tolerance as possible. They have already demonstrated an advance compared to their classical counterparts; increasing qubits is expected to exponentially outpace the classical computers on some tasks. However, not only this, but as we have mentioned, a further study will boost the speed to reach the so-called quantum supremacy.

In order to look at the advantage of NISQ devices, it is fundamental to mention a recent framework which helps exploit the full capabilities of NISQ devices: VQA [17]. This is key to use processes with limited number of qubits, as we will see.

2.1.1 Variational Quantum Algorithms (VQA)

Variational Quantum Algorithms is a framework that encodes a task into a parametrized function run in the quantum computer. All the variational quantum algorithms are based on the Rayleigh-Ritz variational principle, which states that:

$$\min_{\vec{\beta}} \langle \varphi(\vec{\beta}) | H | \varphi(\vec{\beta}) \rangle \geq E_G \tag{2.1}$$

where H is the Hamiltonian of the system and E_G is the ground state energy. The VQA runs the parametrized quantum circuits. And through the measurements from the different variations of the parameter, we perform an analysis on the system.

The concept of VQA is broad. We review one of the most important and simple Variational Quantum algorithms: Variational Quantum Eigensolver.

Variational Quantum Eigensolver

Theoretically, we might be doomed to think that finding the eigenvalue of an operator is an easy task:

$$H |\psi\rangle = E |\psi\rangle$$

In practice, we can see this problem as a phase estimation algorithm, as we can consider the application of an operator as just adding a phase. We can therefore apply the standard quantum phase estimation algorithm to find this value [18]. However, the issue is that an extra number of ancilla qubits are needed to apply this method. Given that extracting the eigenvalue is a fundamental task in quantum computing, a better method is essential for the NISQ devices to operate. Therefore, we trade ancilla qubits for a larger amount of measurements. In fact, VQE requires quadratically more measurements than the phase estimation.

The VQE algorithm serves to find the eigenvalues of a Hamiltonian with just one extra ancilla qubit. This was proven to find the ground state in a particular case in [19]. The procedure is as follows, we first prepare a quantum state $|\psi\rangle$ parametrized by $\vec{\beta}$ to then measure its expectation value $\langle\psi| H |\psi\rangle = \sum_\alpha f_\alpha \left\langle \psi(\vec{\beta}) |\sigma_\alpha| \psi(\vec{\beta}) \right\rangle$ where $\sigma_\alpha = \sigma_1^{\alpha_1} \otimes \sigma_2^{\alpha_2} \otimes \dots \sigma_M^{\alpha_M}$ for M qubits.

The bound that the variational principle provides is the essential point that allows us to iterate to find the eigenvalue. Note that we can decompose the Hamiltonian in terms of the Pauli operators as above, since they form a complete basis of operators. The optimal choice of $\vec{\beta}$ to approximate the ground state is the choice which minimizes the expectation value of H in terms of $\vec{\beta}$. We use non linear optimizer varying the $\vec{\beta}$, such as the gradient based optimizers [20] to find the global minimum which represents the ground state of the system.

One of the risks in the variational algorithms is that associated to optimization techniques. The solution might be confused for a local minimum of the ansatz space. VQA is a very clear representation of the techniques required and used in the algorithms implemented in the experimental settings for NISQ. In fact, VQA is one of the key points of success in our current development of accurate gate implementation [6]

2.2 Quantum noise

We review in this section the general concept of noise, its location, classification and the techniques to alleviate it. In chapter 3, we will specify the error modelling we carry out in our methodology.

Errors affect our computations since they affect the implementation accu-

racy to construct high-quality qubits and gates. This impediment represents a significant challenge to reaching the so-called fault tolerance. The threshold beyond which quantum computers will be considered reliable enough.

If we interpret quantum states as being encoded as wave functions, we can view the concept of quantum noise in terms of errors which arise affecting the interference in the quantum computer. When we construct the quantum states, we are essentially creating a constructive interference to reach the correct answer and destructive interference for any other possibility. Working with interference is very delicate, and two possible types of errors may arise: implementation inaccuracies and interactions with the environment, the latter one being the most significant one. We will classify our errors in that way. Additionally, the location of errors is an interesting point of discussion, as we will next comment on.

2.2.1 Error Location

We can divide the steps of a process in a quantum computer in 3 high-level steps: input, process and output. Due to the qubit limitations in NISQ, we are unable to run algorithms to record where the errors lie in the computer, and hence, it is very difficult to estimate the errors in each step.

However, IBM recent studies estimate that, in their quantum computer, single-qubit gates have an error rate in the range of $0.1\% - 0.3\%$, and two-qubit gates have an error rate in the range of $2\% - 5\%$ [21]. Measurement seems to be the most error-prone operation in current quantum computers. It is also, however, easy to correct as they usually manifest as bit-flip errors. Recent studies have shown an average error rate for measurement operation is in the range of $4\% - 8\%$ and as high as 31% in IBM Machines [21]. We speak more about these in section 3.3.

For the case of initialization errors, it is estimated that the error rate is much lower [22] . Also, other sources claim an accurate initialisation [23].

However, the lack of universality in a quantum computer and the complexity of the noise affecting quantum computers make the results mentioned refer to estimations for specific quantum computers under some specific environmental settings. We must therefore remain cautious and continue to study the error rates in each step of the process.

It has been shown that the implementations of the CNOT gate [24], H

Hadamard [25], Z Phase flip [26] and $\frac{\Pi}{8}$ rotation [27] are still not highly precise. These gates form the universal set and hence their inaccurate implementations means an inaccurate implementation in any gate.
However, recent studies seem to have found ways to implement accurately gates under unitary gate errors and decoherence for single and two qubits [28]. Even though the implementation seems to be accurate, these systems still present some low fidelities [6]. Due to the inability to locate the errors, we are unsure of the source of these or how could we fix them. For this reason, we focus our work on providing a further study on the initialization and measurement errors.
The motivation for this thesis is to explore further how Measurement and Preparation errors affect fidelity in order to predict how this would in principle contribute to the overall fidelity of the process.

2.2.2 Error Classification

To classify the errors, we first define the concept of coherence.

Definition 1 ***Quantum coherence*** *refers to the ability of a quantum state to maintain the superposition state. In quantum computers, quantum states are translated experimentally to be in a high energy state* $|1\rangle$ *or in a low-energy state* $|0\rangle$*.The word coherence, refers to the ability of a quantum mechanical system to build and keep interferences. The loss of coherence is called decoherence, i.e. it is the destruction of the quantum mechanical superposition.*

Definition 2 ***Coherence Time*** *is defined as the time a qubit can retain data. The coherence times for superconducting quantum computers have improved from 1 nano-second to 100 micro-seconds in the last decade [29].*

There are multiple ways to categorize the errors. We classify errors in terms of whether they maintain coherence or not: [30]

Coherence-Errors

Coherent noise is the error that does not destroy the coherence of a state. They are "slow" noise processes, they introduce small perturbations that accumulate and limit the depth of the quantum circuit. These are systematic rotations and are associated with incorrect implementation of the system dynamics.

The coherence error model is achieved via a coherent unitary operation where the target is the desired initial state.

To keep things simple, we view an example. For an incorrect implementation of a quantum circuit, we can find an error induced to be a phase error which creates a small rotation around the X-axis on a state $|0\rangle$, i.e.

$$|\psi\rangle = e^{i\epsilon\sigma_x}|0\rangle = \cos(\epsilon)|0\rangle + i\sin(\epsilon)|1\rangle$$

We wish to obtain the $|0\rangle$ when we measure in the $\{|0\rangle, |1\rangle\}$ basis. However, with the induced error:

$$P(|0\rangle) = \cos^2(\epsilon) \approx 1 - (\epsilon)^2$$
$$P(|1\rangle) = \sin^2(\epsilon) \approx (\epsilon)^2$$

Hence, the probability of error in this trivial quantum algorithm is given by $p_{\text{error}} \approx (\epsilon)^2$, which will be small given that $\epsilon \ll 1$. Here we can see ϵ as an angle that make the error fluctuate from one gate application to another. Usually, all errors are modelled as Pauli errors. However, it was found that coherent errors (systematic rotations) on physical data qubits might also differ significantly from those predicted by a Pauli model [31]. Further than this, even though, coherent errors have been greatly ignored in the literature, recent studies confirm they might be a significant source of noise [32]. This establishes that work around coherent errors is still necessary.

Incoherent-Errors

Incoherent noise is the error that destroys the coherence of a state. This refers to "fast" noise processes and they are described by stochastic errors. This noise on quantum operations sources from the interaction of the quantum system with the environment.
In comparison from above, incoherent errors do not represent systematic errors. We can represent a simple example of how decoherence could act on a initialization state:

$$\rho_i = (1 - p_I)\,|0\rangle\langle 0| + p_I\,|1\rangle\langle 1|$$

where probability p_I is the probability of encountering the initialization error.

Historically, this type of error has been considered the primarily source of noise. We next provide an example of an interaction between state and environment, creating an incoherent noise [33]. We now assume that the environment starts in the pure state, $|E\rangle = |e_0\rangle$, and couples to the system such that:

$$H\sigma_I H|0\rangle|E\rangle = \frac{1}{2}(|0\rangle + |1\rangle)\,|e_0\rangle + \frac{1}{2}(|0\rangle - |1\rangle)\,|e_1\rangle$$

Pure states will be transformed into classical mixtures. Hence, we now move into the density matrix representation for the state $H\sigma_I H|0\rangle|E\rangle$

$$\begin{aligned}\rho_f = &\frac{1}{4}(|0\rangle\langle 0| + |0\rangle\langle 1| + |1\rangle\langle 0| + |1\rangle\langle 1|)\,|e_0\rangle\,\langle e_0| \\ &+ \frac{1}{4}(|0\rangle\langle 0| - |0\rangle\langle 1| - |1\rangle\langle 0| + |1\rangle\langle 1|)\,|e_1\rangle\,\langle e_1| \\ &+ \frac{1}{4}(|0\rangle\langle 0| - |0\rangle\langle 1| + |1\rangle\langle 0| - |1\rangle\langle 1|)\,|e_0\rangle\,\langle e_1| \\ &+ \frac{1}{4}(|0\rangle\langle 0| + |0\rangle\langle 1| - |1\rangle\langle 0| - |1\rangle\langle 1|)\,|e_1\rangle\,\langle e_0|\end{aligned}$$

Since we do not measure the environmental degrees of freedom, we trace over this part of the system, giving,

$$\begin{aligned}\mathrm{Tr}_E\,(\rho_f) &= \frac{1}{4}(|0\rangle\langle 0| + |0\rangle\langle 1| + |1\rangle\langle 0| + |1\rangle\langle 1|) \\ &\quad + \frac{1}{4}(|0\rangle\langle 0| - |0\rangle\langle 1| - |1\rangle\langle 0| + |1\rangle\langle 1|) \\ &= \frac{1}{2}(|0\rangle\langle 0| + |1\rangle\langle 1|)\end{aligned}$$

As we can see, the measurement of the system will consequently return $|0\rangle$ 50% of the time and $|1\rangle$50% of the time. We therefore see the effect of incoherent noise.

An elegant way to formulate both types of errors together is the Lindblad formalism in which the coherent and dynamical evolution of the density matrix can be written as:

$$\partial_t \rho = -\frac{i}{\hbar}[H, \rho] + \sum_k \Gamma_k \mathcal{L}[\rho] \tag{2.2}$$

Where H is the Hamiltonian and $\mathcal{L}_k[\rho] = \left(\left[L_k, \rho L_k^\dagger\right] + \left[L_k\rho, L_k^\dagger\right]\right)/2$ represents the incoherent evolution. The operators L_k are used to model specific decoherence channels, with each operator parametrized by some rate $\Gamma_k \geq 0$. This differential equation is known as the density matrix master equation.

For instance, we can view a bit flip error(incoherent) followed by a rotation error(coherent) on a qubit state ρ as follows:

$$\mathcal{V}_{rotation} \circ \mathcal{V}_{bit-flip}[\rho] = (1-p)e^{-i\epsilon X/2}\rho e^{i\epsilon X/2} + pXe^{-i\epsilon X/2}\rho e^{i\epsilon X/2}X \tag{2.3}$$

where p is the probability of a stochastic bit-flip and ϵ is the angle of a small rotation error that is constant in time.

We can translate our bit-flip and decoherence errors into these parameters to a physical dephasing rate γ and systematic rotation at rate ω through the master equation

$$\frac{d\rho}{dt} = -i\frac{\omega}{2}[X, \rho] + \gamma(X\rho X - \rho) \tag{2.4}$$

by setting $\epsilon = \omega\tau$ and $q = (1 - e^{-2\gamma\tau})/2$ for a gate time τ.

This describes the composition of a coherent process, Λ_ϵ, and an incoherent process, Λ_q. This is a good example for decoherence produced by the environment together with a systematic rotation.

We will next move to describe Quantum Error Correction (QEC) and Quantum Error Mitigation (QEM). Before this, we mention that there has been much more emphasis on QEC and QEM for incoherent errors. However, it is interesting to mention that recently, it has been discovered that [34] when we consider a memory error (qubit decoherence) on a qubit, it has been estimated that the probability of failing is linear with the decoherence time for small errors. In the case of coherent errors, the error probability is estimated to increase quadratically with the decoherence time. Given the fact that QEM and QEC methods are mostly performed for decoherence, there is a concern that coherent errors might be causing unwanted damage due to this quadratic increase in error.

Besides the improvements in the hardware and physical implementations, Quantum Error Correction (QEC) and Quantum Error Mitigation(QEM) are the two possible ways we will reach fault-tolerance: which we will describe next.

But first, we check the three most significant differences and challenges compared to the classical counterpart when battling against errors.

Theorem 1 (No-cloning theorem) *Assume that $|v\rangle$ is a pure (unknown) state. Then there is no unitary operator taking $|v\rangle \otimes |s\rangle$ to $|v\rangle \otimes |v\rangle$ (quantum copy of $|v\rangle$) for all quantum states $|v\rangle$, where $|s\rangle$ is a standard pure state. More precisely, given two particular pure quantum states $|v\rangle$ and $|w\rangle$ to be copied, it follows that the quantum copy process is possible only if $|v\rangle = |w\rangle$ or if $|v\rangle$ and $|w\rangle$ are orthogonal.*

In addition, the set of errors is continuous and so, at first glance, it seems that the quantum code must correct an infinity of errors. Unlike for the classical case, in which a bit can only take values of 0 or 1 and the error is limited. The third difficulty is that the measurements of qubits destroy the quantum information, and therefore we must minimise our measurements.

These are three conditions that establish the limits to our work. We have to work around these to formulate our solutions to aid our quantum algorithms against noise.

2.2.3 Quantum Error Correction

It is the ideal way to solve the issues with errors. Classical and Quantum computers require at least some form of error correction. Quantum Error Correction is comparable to classical Error Correction [35].

Experimentally, it has only been recently when QEC [36] [2] has provided with fault-tolerance in one logical qubit i.e one data qubit and 8 ancilla qubits. In this code, more errors are suppressed than introduced by the overhead required to implement the error correction. This was a recent work of the Google team. They applied QEC and claimed to have error rates as low as 10^{-15} [2], in comparison to other state-of-the-art quantum platforms that typically have physical error rates near 10^{-3} [37] [38] [39] [40]

To provide an example of how QEC is performed we explain the method carried out by Google.

In general, the idea behind a stabilizer code [41] is that quantum states could be represented by operators that stabilize them, e.g. $|\psi\rangle = (|00\rangle + |11\rangle)/\sqrt{2}$ is the unique state such that

$$\boldsymbol{X}_1\boldsymbol{X}_2|\psi\rangle = |\psi\rangle, \quad \boldsymbol{Z}_1\boldsymbol{Z}_2|\psi\rangle = |\psi\rangle$$

QEC makes use of this concept to identify errors to then correct them. It also uses the following key mathematical terms:

1. Pauli Group: refers to $\mathbb{G}_n = \{\boldsymbol{I}, \boldsymbol{X}, \boldsymbol{Y}, \boldsymbol{Z}\}^{\otimes n} \otimes \{\pm 1, \pm i\}$ with properties: $P^2 = \pm I, \quad PQ = \pm QP, \quad PP^\dagger = I$

2. Stabilizer group S: it is a subgroup of $\mathbb{G}_n$ in which all elements commute with each other. It does not contain $-\boldsymbol{I}$.

3. Stabilizer generators: are the minimal set of operators $\boldsymbol{g_k}$ that generate $S : \mathscr{S} =< \boldsymbol{g}_1, \boldsymbol{g}_2, \cdots, \boldsymbol{g}_r > \subseteq \mathbb{G}_n$

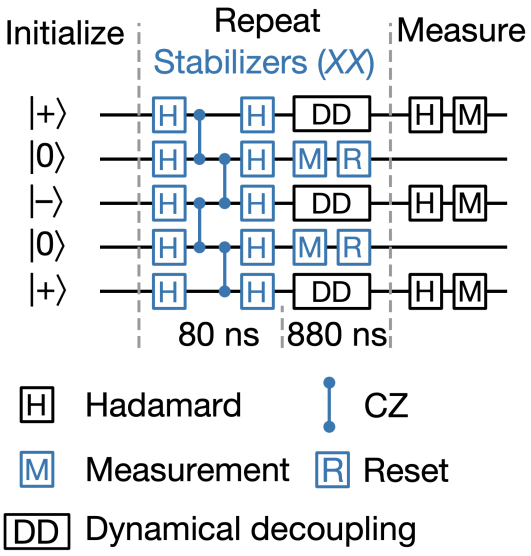

Figure 2.2: Schematic visualization of the circuit Google implemented for phase-flip error correction code in their quantum computer [2].

4. Stabilizer subspace: is the subspace of dimension 2^{n-r}

$$\mathcal{H}_S = \{|\psi\rangle | \boldsymbol{S}|\psi\rangle = |\psi\rangle \text{ for } \boldsymbol{S} \in \mathbb{S}\}$$

Also, we enunciate the conditions for the correction of errors. Suppose $\{E_k\}$ is a set of operators in $\mathbb{G}_n$ and $\mathbb{S}$ is the stabilizer for a quantum code. The error can be corrected if:

- $\boldsymbol{E}_a^\dagger \boldsymbol{E}_b \in \mathbb{S}$
- There is an $\boldsymbol{M} \in \mathbb{S}$ that anti-commutes with $\boldsymbol{E}_a^\dagger \boldsymbol{E}_b$.

We can show a small proof as follows:

Case 1: $\langle \phi_j | \boldsymbol{E}_a^\dagger \boldsymbol{E}_b | \phi_{\boldsymbol{k}} \rangle = \langle \phi_j \mid \phi_{\boldsymbol{k}} \rangle = \delta_{jk}$

Case 2: $\langle \phi_j | \boldsymbol{E}_a^+ \boldsymbol{E}_b | \phi_k \rangle = \langle \phi_j | \boldsymbol{E}_a^\dagger \boldsymbol{E}_b \boldsymbol{M} | \phi_k \rangle = - \langle \phi_j | \boldsymbol{M} \boldsymbol{E}_a^\dagger \boldsymbol{E}_b | \phi_k \rangle = - \langle \phi_j | \boldsymbol{E}_a^\dagger \boldsymbol{E}_b | \phi_k \rangle$ and therefore $\langle \phi_j | \boldsymbol{E}_a^\dagger \boldsymbol{E}_b | \phi_k \rangle = 0$

Hence, given a circuit as the one in the figure 2.2, for a stabilizer code with generators $< \boldsymbol{g}_1, \boldsymbol{g}_2, \cdots, \boldsymbol{g}_r >$: if we measure all the generators and each of the measurements yields $+1$, we know that our logical qubit's state

belongs to the code subspace. Otherwise, if a measurement yields -1, we can conclude that an error has happened. We can then apply a phase-flip to correct it.

The main complication with QEC is not being able to create as many qubits as required. Even if we did, we would never reach an infinite correction given that we can see errors as continuous. This means that more techniques to reduce noise are also required.

2.2.4 Quantum Error Mitigation

The importance of QEM for our work is in different ways. Primarily, it first helps us put our work into context. The effectiveness of QEM techniques, together with VQA, to implement quantum gates is what has sparked our interest in the topic of this thesis. Beyond this, QEM is the main space in which we hope our discoveries could be utilised. As we will see, it is fundamental to have extensive knowledge of the errors and the error rates to apply mitigation techniques to them.

Quantum Error Mitigation (QEM) are methods that aim to reduce errors in quantum processes without the use of extra qubits. They employ **hybrid quantum-classical algorithms** [42] to perform classical post-processing optimisation of the experiment data of the quantum process. Their target is to estimate what the outcome would have been if the noise was not present.

QEM is a very popular subject of recent studies, e.g. [43]. Currently, all the available quantum computers run these hybrid quantum-classical algorithms to be able to reach a quantum advantage [44].

To start with, we can look at a very simple error mitigation case, in order to exemplify what QEM tries to perform. When we want to reconstruct a matrix from an erroneous one, we can build a correlation matrix with the errors: $p_{exp} = Cp_{ideal}$. After we have obtained this correlation matrix, we can correct all our future calculations with the aid of this matrix. The effectiveness of this method relies on 2 main assumptions: the number of experiments we perform is very large and that the noise model is constant. This is an elegant linear inversion method, however, experimentally, we need to look for more sophisticated techniques that could offer us an advantage in a less ideal scenario.

Hence to further explore how quantum error mitigation is performed, we

review one of the current noise reduction techniques. Before this, we define the concept of POVM that we will use across our method.

Definition 3 (Positive operator-valued measure) *A positive operator-valued measure (POVM) is defined by a set of operators* $\{P_k\}$ *satisfying the completeness condition:* $\sum_k P_k^\dagger P_k = I$*, where each* P_k *is a POVM element.* $\{P_i\}$ *is also positive semi-definite i.e.*

$$\mathbf{x}^\top P\mathbf{x} \geq 0$$

for all $\mathbf{x} \in \mathbb{R}^n \backslash \{\mathbf{0}\}$(2.5)

In contrast to projective measurements, A POVM is the mathematical concept that defines a generalised measurement. It is introduced to prevent mistakes from possible new representations and manipulations of measurements. For a system in state ρ, the result represented by operator P will occur with probability $\mathrm{Tr}(\rho P)$. In fact, in terms of POVM, we can see that QEM methods target at recovering the expectation value of observables, which translates as recovering $<P> = Tr(\rho_{ideal} P)$.

Linear Extrapolation Error Mitigation

For an expectation value $E(\lambda) =< P >$, suppose we can expand the noisy expectation value as a Taylor series as follows:

$$E^{(d)}_{\text{poly}}(\lambda) = a_0 + a_1\lambda + \dots a_d\lambda^d \tag{2.6}$$

where λ is the noise strength and the parameters a_i are real parameters. a_0 represents the noiseless expectation value. If we only consider the case of $d = 1$, we refer to this as linear extrapolation. The main point on the extrapolation technique is that, considering we can manipulate the noise scale for n noise rates $\lambda_j = c_j\lambda$ in which $c_0 = 1 < c_1 < c_2 \dots < c_n$, and obtain a set of their corresponding measurements $\mathbf{y} = \{y_1, y_2, \dots y_n\}$: we can find an analytic solution computing the classical optimization least squares estimation technique, which gives the following result:

$$E(0) = \frac{1}{m}\sum_j y_j - \frac{\sum_j \left(\lambda_j - \bar{\lambda}\right)\left(y_j - \frac{1}{m}\sum_j y_j\right)}{\sum_j \left(\lambda_j - \bar{\lambda}\right)^2}\bar{\lambda}$$

where $\bar{\lambda} = \frac{1}{m}\sum_j \lambda_j$

Note that the manipulation on the error rate can be carried out by re-scaling parameters in our system. See [43] for more details.

We note that we have "extrapolated" the erroneous term. In this case, it was only one term. However, the extrapolation technique can be expanded for more errors terms. When $a_d \neq 0$ for d=0,1,2 it takes the name of Richardson extrapolation. The noiseless expectation value is calculated through the interpolating Lagrange polynomial.

Our research hopes to help understand the effectiveness of the error mitigation techniques. As we will see, our model takes an error and assesses how it would affect a process. We can therefore use this methodology to compare theoretically the quality of the dynamics in the presence of the error against the case in which the error is mitigated. Another important note to take-away is that the knowledge on the error is key to optimize our error mitigation techniques, as they mostly rely on a good choice of ansatz. This is also something we contribute to, as we are helping expand the knowledge on the effect of errors.

Together with VQA, Error mitigation techniques have proven to be very effective in the accurate implementation of quantum gates, as we have previously mentioned [6].

2.3 Quantum Tomography

Quantum Tomography is the mathematical description to reconstruct the different parts of a quantum information process. There has been different methods of performing tomography. We note that one of the main mathematical concepts used in Quantum Tomography is the Born rule, $p_\mu = Tr(P_\mu \Lambda[\rho])$ for a channel Λ and a projector P_μ [45].

2.3.1 Quantum State Tomography

Quantum State Tomography (QST) is the technique to reconstruct quantum states through the measurement of different outputs. The importance of QST is to obtain an estimation of the state without having to perform a measurement directly affecting our quantum circuit.

QST Classical Analog

A nice example to view the meaning of Quantum State Tomography is to find its classical equivalent. The simplest analogy is to estimate the bias of a coin [46].

For a certain bias p, we model the coin toss as a random variable CT with outcomes 1 for Heads and 0 for Tails. The probability distribution corresponds to: $\Pr(CT \mid p) = p^{CT}(1-p)^{1-CT}$. For n_{Tot} independent measurements and we get n_{H} heads then the estimated bias of the coin is

$$p_{\text{estimated}} = \frac{n_H}{n_{\text{Tot}}}$$

We take the bias to be the density matrix representing the state of the qubit, the random variable is the measurement.

Following this introduction, we describe the most important method for QST: Direct Inversion Tomography. Before we work through this method, we will clarify a few important concepts:

Definition 4 (Bloch sphere state) *We can describe the most general state of a qubit as a superposition of states*

$$a\,|1\rangle + b\,|0\rangle$$

A point $(a, b) \in C^2$ fulfill this condition iff it lies on the Bloch Sphere. A reasonable parametrization is given by $a = e^{i\lambda}\cos\left(\frac{\theta}{2}\right), b = e^{i\lambda}\sin\left(\frac{\theta}{2}\right)e^{i\phi}$, where a and b are complex numbers. The overall phase factor λ has no observable effect and can be set to zero. The variables $\theta \in [0, \Pi]$ and $\phi \in [0, 2\Pi]$ are numbers that define a point on the surface of the Bloch sphere. We note that the bloch sphere only represents pure states.

For an operation Λ, the isomorphism $\mathrm{SU}(2) \cong \mathrm{SO}(3)/1$ gives the possibility to see this operation on the qubit as a simple rotation of its Bloch vector in R^3, where the eigenstates of Λ are equal to the rotations axis. The advantage is clear: abstract operations in the special unitary space became now simple rotations in the three dimensional space. Note that this is considered for a system that is not under a dephasing process.

Definition 5 (Rotation operators on the Bloch Sphere) *The rotation operators on the Bloch sphere about the axes x, y and z by angle ϕ are described by:*

$$R_x^\theta \equiv e^{-i\theta\sigma_x/2} = \cos\left(\frac{\theta}{2}\right) I - i\sin\left(\frac{\theta}{2}\right)\sigma_x = \begin{pmatrix} \cos\frac{\theta}{2} & -i\sin\frac{\theta}{2} \\ -i\sin\frac{\theta}{2} & \cos\frac{\theta}{2} \end{pmatrix} \quad (2.7)$$

$$R_y^\theta \equiv e^{-i\theta\sigma_y/2} = \cos\left(\frac{\theta}{2}\right) I - i\sin\left(\frac{\theta}{2}\right)\sigma_y = \begin{pmatrix} \cos\frac{\theta}{2} & -\sin\frac{\theta}{2} \\ \sin\frac{\theta}{2} & \cos\frac{\theta}{2} \end{pmatrix} \quad (2.8)$$

$$R_z^\theta \equiv e^{-i\theta\sigma_z/2} = \cos\left(\frac{\theta}{2}\right) I - i\sin\left(\frac{\theta}{2}\right)\sigma_z = \begin{pmatrix} e^{-i\theta/2} & 0 \\ 0 & e^{i\theta/2} \end{pmatrix} \quad (2.9)$$

We note that using the Bloch sphere to more than one qubit becomes complicated. However, since we build our method from the 1-qubit case, this is still very useful.

Definition 6 (Pure density operator) *For the system of N qubits the pure density operator is a $2^N \times 2^N$ matrix that contains $\left(4^N - 1\right)$ independent real parameters. The density matrix can be written as:*

$$\hat{\rho} = \begin{pmatrix} \rho_{00} & \rho_{01} \\ \rho_{10} & \rho_{11} \end{pmatrix} = \rho_{00}|0\rangle\langle 0| + \rho_{01}|0\rangle\langle 1| + \rho_{10}|1\rangle\langle 0| + \rho_{11}|1\rangle\langle 1| \quad (2.10)$$

or explicitly as

$$\hat{\rho} = |\Psi\rangle\langle\Psi| = |a|^2 \mid 0\rangle\langle 0| + ab^*|0\rangle\langle 1| + a^*b|1\rangle\langle 0| + |b|^2 \mid 1\rangle\langle 1| \quad (2.11)$$

$$= \begin{pmatrix} |a|^2 & ab^* \\ a^*b & |b|^2 \end{pmatrix}$$

Also, the density operator satisfies:

- *Hermitian:* $\rho = \rho^\dagger$
- *Unity trace:* $\mathrm{Tr}(\rho) = 1$

Definition 7 (Bloch vector $\hat{r}$) *We can see that the definition of ρ can be easily inverted and the coefficients of the Bloch vector can be expressed as:*

$$\begin{aligned} r_x &= \rho_{01} + \rho_{10} = 2\,\mathrm{Re}\,(\rho_{10}) \\ r_y &= i\,(\rho_{01} - \rho_{10}) = 2\,\mathrm{Im}\,(\rho_{10}) \\ r_z &= \rho_{00} - \rho_{11} = 1 - 2\rho_{11} \end{aligned} \quad (2.12)$$

Once defined these concepts, we move to look at the Direct Inversion Tomography method.

Direct Inversion Tomography

Our aim is to obtain the Bloch vectors describing our state $|\psi\rangle$.

From a similar way to the classical case, we encode it through the expectation value. If we take a measurement in $|1\rangle\langle 1|$, considering a large amount of experiments, we obtain $p_z = |\langle 1 \mid \psi\rangle|^2$, which we can expand as follows:

$$p_z = |\langle 1 \mid \psi\rangle|^2 = |b|^2 = \sin^2\left(\frac{\theta}{2}\right) = \frac{1-\cos(\theta)}{2} = \frac{1-r_z}{2}$$

where p_z is the average of the experiments. From this expansion we see we obtain r_z.

From the definition of r_z in terms of ρ_{11}, we can calculate the rest of the coefficients by rotating.

Rotating $\theta = \frac{\pi}{2}$ about x-axis, yields the imaginary part of the element ρ_{10} of the density matrix (note that $\mathrm{Im}(\rho_{10}) = -\mathrm{Im}(\rho_{01})$), because after this rotation the r_y-coefficient of the Bloch vector appears to be in front of the σ_z-matrix in the Pauli decomposition of the density matrix:

$$R_x^\theta \hat{\rho} \left(R_x^\theta\right)^\dagger = \begin{pmatrix} \cos(\theta/2) & -i\sin(\theta/2) \\ -i\sin(\theta/2) & \cos(\theta/2) \end{pmatrix} \hat{\rho} \begin{pmatrix} \cos(\theta/2) & i\sin(\theta/2) \\ i\sin(\theta/2) & \cos(\theta/2) \end{pmatrix} |_{\theta=\pi/2} =$$
$$= \left(r_0\sigma_0 + r_x\sigma_x - r_z\sigma_y + r_y\sigma_z\right)/2$$

because

$$R_x^{\pi/2}\sigma_x \left(R_x^{\pi/2}\right)^\dagger = \sigma_x, \quad R_x^{\pi/2}\sigma_y \left(R_x^{\pi/2}\right)^\dagger = \sigma_z, \quad R_x^{\pi/2}\sigma_z \left(R_x^{\pi/2}\right)^\dagger = -\sigma_y$$

Analogously, after rotation by the angle $\theta = -\pi/2$ about y-axis, yields the coefficient r_x of the Bloch vector (now under this rotation the coefficient r_x appears to be in front of the σ_z-matrix), and, therefore, $\mathrm{Re}(\rho_{10})$ element of the density matrix is measured:

$$R_y^\theta \hat{\rho} \left(R_y^\theta\right)^\dagger = \begin{pmatrix} \cos(\theta/2) & -\sin(\theta/2) \\ \sin(\theta/2) & \cos(\theta/2) \end{pmatrix} \hat{\rho} \begin{pmatrix} \cos(\theta/2) & \sin(\theta/2) \\ -\sin(\theta/2) & \cos(\theta/2) \end{pmatrix} \Big|_{\theta=-\pi/2} =$$
$$= \left(r_0\sigma_0 - r_z\sigma_x + r_y\sigma_y + r_x\sigma_z\right)/2$$

because

$$R_y^{-\pi/2}\sigma_x \left(R_y^{-\pi/2}\right)^\dagger = \sigma_z, \quad R_y^{-\pi/2}\sigma_y \left(R_y^{-\pi/2}\right)^\dagger = \sigma_y, \quad R_y^{-\pi/2}\sigma_z \left(R_y^{-\pi/2}\right)^\dagger = -\sigma_x$$

We therefore see we can provide the full characterisation of the density matrix. For multiple qubits, the expansion of the density matrix in terms of Pauli matrices can be generalized to $\hat{\rho} = \frac{1}{2^N} \sum_{i=0}^{3} \sum_{j=0}^{3} \ldots \sum_{k=0}^{3} r_{ij\ldots k} \sigma_i \otimes \sigma_j \otimes \ldots \otimes \sigma_k$, and the idea of the measurement remains the same: measure some coefficients $r_{ij\ldots k}$, apply basis rotations, and measure other coefficients r.

We require 3^N rotations to perform QST. For a single qubit we only require 3 rotations (counting with the identity rotation), for 2 qubits we require a nine and for 3 qubits we require twenty seven.

2.3.2 Quantum Process Tomography

Quantum Process Tomography (QPT) is the procedure to characterize an unknown quantum process [47]. This methodology requires the preparation of a set of quantum states. We then evolve these quantum states with the unknown quantum process and proceed to measure them. Once we have the information about the input and output states, we can now reconstruct the gate, and often we need to choose a suitable estimation procedure to reconstruct the gate.

In this section, we will present two of the most relevant different approaches to QPT, direct and indirect dynamics characterisation. We refer to "direct" to those who do not require QST in the characterization of the dynamics, "indirect" if they do.

Before discussing these methods, we point out several mathematical concepts we will come across.

Firstly, we define the operator-sum representation of our linear map as:

$$\mathcal{E}(\rho) = \sum_{i}^{d^2} \bar{A}_i \rho \bar{A}_i{}^{\dagger} \tag{2.13}$$

where $d = 2^N$ is the dimension of the system and N is the number of qubits. $\bar{A}_i$ are the so-called Kraus operators. The Kraus Operators for a complete positive trace preserving (CPTP) [1] linear map satisfy the completeness relation:

$$\sum_i A_i^{\dagger} A_i = 1$$

This ensures that ρ remains hermitian trace one (i.e. the map is trace preserving) . Proof:

$$1 = \operatorname{Tr} \mathcal{E}(\rho) = \operatorname{Tr}\left(\sum_j \bar{A}_j \rho \bar{A}_j{}^{\dagger}\right) = \sum_j \operatorname{Tr}\left(\bar{A}_j \rho \bar{A}_j{}^{\dagger}\right) = \operatorname{Tr}\left(\sum_j \bar{A}_j{}^{\dagger} \bar{A}_j \rho\right)$$

This means that we can write the effect of the map as $\rho \to \mathcal{E}(\rho)$.

[1] Note that a linear map $\Lambda : A \to B$ is called positive map if Λ maps positive elements to positive elements: $a \geq 0 \Longrightarrow \Lambda(a) \geq 0$.
we extend this to complete positive in the following way: $\forall |\phi\rangle \in H_A \otimes H_B$: $\langle \phi | \Lambda_A \otimes 1 (\rho_{AB}) | \phi \rangle \geq 0$

In case of a non trace preserving quantum operation, the condition becomes $\sum_{j=1}^{K} \bar{A_j}^{\dagger} \bar{A_j} \leq I$

We may further expand Equation 2.13 in terms of a basis A_β together with a classical error correlation matrix χ such that:

$$\mathcal{E}(\rho) = \sum_{\alpha,\beta=1}^{d^2} \chi_{\alpha\beta} A_\alpha \rho A_\beta^\dagger \tag{2.14}$$

$\chi \in \mathbb{C}^{d^2 \times d^2}$ is the process matrix and $A_\alpha \in \mathbb{C}^{d \times d}$ is a chosen basis of operators.

For the one qubit case, χ will have 12 independent parameters. And if we take the Pauli Operators to be our basis operators, we can see the error correlation matrix terms in the following way:

- 3 of these describe arbitrary unitary transforms $\exp\left(i \sum_k r_k \sigma_k\right)$ on the qubit
- 9 parameters describe possible correlations established with the environment E via $\exp\left(i \sum_{jk} \gamma_{jk} \sigma_j \otimes \sigma_k^E\right)$

An important note is that by assuming that the map is trace preserving, χ reduces from d^4 to $d^4 - d^2$ real independent parameters [47]

Standard Quantum Process Tomography

In summary, we require of a tomographically complete sets of input states $\{\rho_1, \ldots, \rho_N\}$ and POVM $\{P_1, \ldots, P_N\}$. Then, by relating the equation 2.14 to $\vec{p}^{\,\text{exp.}}$:

$$\vec{p}^{\,\text{exp.}} = \text{Tr}\left(P_i \mathcal{E}\left(\rho_k\right)\right) = \sum_{\alpha,\beta} \text{Tr}\left(P_i A_\alpha \rho_k A_\beta^\dagger\right) \chi_{\alpha\beta}$$

We can linearly invert and find the matrix χ, which thus defines uniquely the process matrix. We will review this method in detail in chapter 3

We must also mention that the other popular Indirect QPT method is AAPT [48] but we will not expand on this method.

Direct characterization of quantum dynamics (DCQD)

Direct characterization of quantum dynamics (DCQD) is a direct gate reconstruction technique [49]. It relies on the error-detection stabilizer formalism instead of QST. Here, we explain briefly how this method works for one qubit, but we note that this method can be expanded to a larger number of qubits. To do this, we must embed the system in a k-prime dimensional Hilbert Space, as we can see in the publication [49]

If we recall our definition for CPTP maps, we can see that we expand these in terms of Pauli Operators and a matrix χ. For one qubit, if we maximally entangle 2 qubits as $|\psi\rangle = (|0_A 0_B\rangle + |1_A 1_B\rangle)/\sqrt{2}$, and then subject only qubit A to a map $\mathcal{E}$, we see that the basis $\{A_\alpha\}_{\alpha=0}^{3}$ becomes the identity operator and the Pauli operators: $\{I, X, Y, Z\}$. This then means that the state $|\psi\rangle$ is stabilized by $Z^A Z^B$ and $X^A X^B$. Hence if we measure for the stabilizers using an appropriate set of 4 projection operators, we can obtain the corresponding elements in $\chi_{\alpha\alpha}$ with the relation: $p_\alpha = \mathrm{Tr}\left[P_\alpha \mathcal{E}(\rho)\right] = \chi_{\alpha\alpha}$.

The other elements of χ are calculated using this same concept. We take the following table from [49] to present how the method is applied to a 1 qubit case:

input state	Measurement		output
	Stabilizer	Normalizer	
$(\|0\rangle\|0\rangle + \|1\rangle\|1\rangle)/\sqrt{2}$	$Z^A Z^B, X^A X^B$	N/A	$\chi_{00}, \chi_{11}, \chi_{22}, \chi_{33}$
$\alpha\|0\rangle\|0\rangle + \beta\|1\rangle\|1\rangle$	$Z^A Z^B$	$X^A X^B$	χ_{03}, χ_{12}
$\alpha\|+\rangle\|0\rangle + \beta\|-\rangle\|1\rangle$	$X^A Z^B$	$Z^A X^B$	χ_{01}, χ_{23}
$\alpha\|+i\rangle\|0\rangle + \beta\|-i\rangle\|1\rangle$	$Y^A Z^B$	$Z^A X^B$	χ_{02}, χ_{13}

Note that for the off-diagonal set of elements, we also exploit the concept of Normalizer. We can see a detailed explanation on the topic in [50].

An interesting fact about DCQD is that we can also apply this technique partially to obtain partial information about the process. This is key for those circumstances in which we have some extra knowledge on the dynamics or also when we do not need the full details of the process.

2.4 Fidelity

Under the presence of errors it is fundamental to have a good understanding of the quality of the process to measure its reliability. We find a convenient way to estimate this is through gate fidelity. We will use this resource to compare the gate we want to implement against the gate reconstructed via QPT. This will provide us with a way to measure the impact of the errors in our process.

To compare two items of information, we can make use of "distance measures" [51]. We can measure the distance of two quantum states or processes by either trace distance[2] or fidelity. Nielsen exploited this concept to define Gate fidelity, and he first defined it to be as follows

For a quantum channel described by a trace-preserving quantum operation, $\mathcal{E}$, the average gate fidelity is defined by

$$\bar{F}(\mathcal{E}) \equiv \int d\psi \langle\psi|\mathcal{E}(\psi)|\psi\rangle$$

where the measure $d\psi$ is on state space, normalized so $\int d\psi = 1$.

You can find more specifics on the definition in the paper. Note that ψ indicates either $|\psi\rangle$ or $|\psi\rangle\langle\psi|$.

However, for this thesis, we are interested in the measure of how well $\mathcal{E}$ approximates a quantum gate, U,

$$\bar{F}(\mathcal{E}, U) \equiv \int d\psi \left\langle \psi \left| U^\dagger \mathcal{E}(\psi) U \right| \psi \right\rangle$$

Note that $F(\mathcal{E}, U) = 1$ if and only if $\mathcal{E}$ implements U perfectly, while lower values indicate that $\mathcal{E}$ is a noisy implementation of U. Note that $\bar{F}(\mathcal{E}, U) = \bar{F}\left(\mathcal{U}^\dagger \circ \mathcal{E}\right)$, where $\mathcal{U}^\dagger(\rho) \equiv U^\dagger \rho U$.

There is other fidelities we can take into account like state fidelity. State fidelity is a measure of the difference between the state we have and the state we would like to have, for any single or multi qubit quantum system. This is useful when we use Quantum state tomography as a mean to characterise the actual state. State fidelity estimates the proximity between the tomographic state and the target [52].

There are many other methods to estimate fidelity. Usually the calculation of fidelity is very costly, so estimations of fidelity are required. Recently, there has been many advances in this space, given its importance as it provides us with a way to measure how well our system is implemented.

[2]Trace is the trace norm of the difference of the matrices $T(\rho, \sigma) := \frac{1}{2}\|\rho - \sigma\|_1$

We note that the biggest point for discomfort that fidelity brings is that the experimental calculation is very bothersome since it requires a change of set up at every part of the experiment. We see that an alternative version of fidelity have been developed in [6] in which we introduce estimations to remove experimental steps. These new techniques have proven to be a faithful approximation, specially for high fidelities.

Chapter 3

SQPT implementation with noise on 1 and 2 qubits

In this section, we discuss the main work of our research. We can divide it in three parts: building the appropriate QPT method, modelling the adequate errors and assessing the fidelity of the QPT under these errors. We use SQPT as the QPT method. Even though DCQD reduces considerably the number of measurements , we note that DCQD uses a larger Hilbert space, compared to that of SQPT. It is for this reason that we will take SQPT in our research, since we are considering methods that could be performed with a small number of qubits i.e. for NISQ devices. Besides this, SQPT offers a very simple linear inversion method which makes the insertion of the errors clearer. In terms of noise, we use incoherent noise to model the initialization and measurements errors. To assess fidelity, we use gate fidelity in terms of the error matrix χ. The main goal of this study is to develop an artifact to measure the effect of input and output errors in fidelity. Our method is implemented for one and two qubits. All this work has been formulated in Mathematica and the code is available at: https://github.com/isabelfrancg/Fidelity-study

3.1 One qubit implementation

First, we will walk through the implementation of SQPT. We use SQPT to reconstruct a CPTP process, given an input and measurement. SQPT is a very good method theoretically for the 1 and 2 qubit channels, but requires of other techniques beyond that. We will speak more in detail about this in section 4.
As explained in Section 2.3 if we have a CPTP channel, it can be written in

the following way:

$$\Lambda(\varrho) = \sum_{ij} \chi_{ij} \sigma_i \varrho \sigma_j^\dagger \ . \tag{3.1}$$

SQPT aims to calculate the error matrix χ through the measurements of the probabilities:

$$p_{ij} = \mathrm{Tr}\left(P_i \Lambda(\varrho_j)\right) \tag{3.2}$$

These probabilities are the measurement outcomes after applying the channel to a complete set of states ϱ_j. We find their relation to χ_{pq} via the expression:

$$p_{ij} = \sum_{pq} \chi_{pq} \mathrm{Tr}\left(P_i \sigma_p \varrho_j \sigma_q^\dagger\right) \tag{3.3}$$

of linear equations. We can simplify the right hand side by defining:

$$A_{ijpq} = \mathrm{Tr}\left(P_i \sigma_p \varrho_j \sigma_q^\dagger\right) \tag{3.4}$$

If we introduce a single index $\alpha = \alpha(i,j)$ for the double index i,j, and similarly β for p,q, then A becomes a matrix, and the vector $\vec{\chi}$ with elements χ_β reads

$$\vec{\chi} = A^{-1}\vec{p} \tag{3.5}$$

We note that for the one qubit case $p_{ij}, i \in \{1,4\}$ and $j \in \{1,4\}$ which corresponds to the number of measurements we require. In total, 16 measurements.

Flattening the p_{ij} matrix makes a p_α, which is a 16x1 matrix. For the case of A_{ijpq} it is a 16x16 matrices. A counts with 256 elements. We note that the calculation of A is costly, however, it is only required once. We can reuse its value for different processes, if we use the same type of projectors and initialization states. So in our case, we do recycle this value for all gates in the one qubit case.

In particular we look at the representation of A as follows:
We show $A_{ijpq} =$

$$\begin{pmatrix} \mathrm{Tr}(\rho_1\sigma_p\rho_1\sigma_q^\dagger) & \mathrm{Tr}(\rho_1\sigma_p\rho_2\sigma_q^\dagger) & \mathrm{Tr}(\rho_1\sigma_p\rho_3\sigma_q^\dagger) & \mathrm{Tr}(\rho_1\sigma_p\rho_4\sigma_q^\dagger) \\ \mathrm{Tr}(\rho_2\sigma_p\rho_1\sigma_q^\dagger) & \mathrm{Tr}(\rho_2\sigma_p\rho_2\sigma_q^\dagger) & \mathrm{Tr}(\rho_2\sigma_p\rho_3\sigma_q^\dagger) & \mathrm{Tr}(\rho_2\sigma_p\rho_4\sigma_q^\dagger) \\ \mathrm{Tr}(\rho_3\sigma_p\rho_1\sigma_q^\dagger) & \mathrm{Tr}(\rho_3\sigma_p\rho_2\sigma_q^\dagger) & \mathrm{Tr}(\rho_3\sigma_p\rho_3\sigma_q^\dagger) & \mathrm{Tr}(\rho_3\sigma_p\rho_4\sigma_q^\dagger) \\ \mathrm{Tr}(\rho_4\sigma_p\rho_1\sigma_q^\dagger) & \mathrm{Tr}(\rho_4\sigma_p\rho_2\sigma_q^\dagger) & \mathrm{Tr}(\rho_4\sigma_p\rho_3\sigma_q^\dagger) & \mathrm{Tr}(\rho_4\sigma_p\rho_4\sigma_q^\dagger)) \end{pmatrix} \tag{3.6}$$

for the case $i = a$ and $j = b$, $\rho_a \sigma_p \rho_b \sigma_q^\dagger =$

$$\begin{pmatrix} \rho_a\sigma_1\rho_b\sigma_1^\dagger & \rho_a\sigma_1\rho_b\sigma_2^\dagger & \rho_a\sigma_1\rho_b\sigma_3^\dagger & \rho_a\sigma_1\rho_b\sigma_4^\dagger \\ \rho_a\sigma_2\rho_b\sigma_1^\dagger & \rho_a\sigma_2\rho_b\sigma_2^\dagger & \rho_a\sigma_2\rho_b\sigma_3^\dagger & \rho_a\sigma_2\rho_b\sigma_4^\dagger \\ \rho_a\sigma_3\rho_b\sigma_1^\dagger & \rho_a\sigma_3\rho_b\sigma_2^\dagger & \rho_a\sigma_3\rho_b\sigma_3^\dagger & \rho_a\sigma_3\rho_b\sigma_4^\dagger \\ \rho_a\sigma_4\rho_b\sigma_1^\dagger & \rho_a\sigma_4\rho_b\sigma_2^\dagger & \rho_a\sigma_4\rho_b\sigma_3^\dagger & \rho_a\sigma_4\rho_b\sigma_4^\dagger \end{pmatrix} \tag{3.7}$$

As we did for p_{ij}, we flatten A_{ijpq} to $A_{\alpha\beta}$ such that we obtain a 16x16 matrix.

Finally, we can obtain the χ_{pq} matrix:

$$\begin{pmatrix} p_{11} \\ p_{12} \\ ... \\ p_{21} \\ ... \\ p_{44} \end{pmatrix} \cdot \begin{pmatrix} A_{1111} & ... & A_{1114} & A_{1211} & ... & A_{1414} \\ A_{1121} & ... & A_{1124} & A_{1221} & ... & A_{1424} \\ ... & ... & ... & ... & ... & ... \\ A_{2111} & ... & A_{2114} & A_{2211} & ... & A_{2414} \\ ... & .... & ... & ... & ... & ... \\ A_{4141} & ... & A_{4144} & A_{4241} & ... & A_{4444} \end{pmatrix}^{-1} \tag{3.8}$$

Finally, we reconstruct the gate by performing the summation in Equation 3.1.

We note that our measurement of the probabilities p_{ij} is through the choice of the following complete set of initialization and projector states:

$$\varrho_1 = P_1 = |0\rangle \langle 0| \tag{3.9}$$

$$\varrho_2 = P_2 = |1\rangle \langle 1| \tag{3.10}$$

$$\varrho_3 = P_3 = |x\rangle \langle x| \ , \text{ with } |x\rangle = \frac{1}{\sqrt{2}}(|0\rangle + |1\rangle) \tag{3.11}$$

$$\varrho_4 = P_4 = |y\rangle \langle y| \ , \text{ with } |y\rangle = \frac{1}{\sqrt{2}}(|0\rangle + i\,|1\rangle) \ , \ \langle y| = \frac{1}{\sqrt{2}}(\langle 0| - i\,\langle 1|) \tag{3.12}$$

Next, we check how we introduce errors in our SQPT technique

General form of errors for one qubit SQPT

We note that errors we consider in SQPT will have the following form:

Initialization Error

The initialization errors get introduced in our work in the following way:

$$p_{i1} = Tr(P_i\Lambda(\rho_1^{error})) = (p[Tr(P_i\Lambda(|0\rangle\langle 0|))] + (1-p)[Tr(P_i\Lambda(\delta_1))]) \quad (3.13)$$

$$p_{i2} = Tr(P_i\Lambda(\rho_2^{error})) = (p[Tr(P_i\Lambda(|1\rangle\langle 1|))] + (1-p)[Tr(P_i\Lambda(\delta_2))]) \quad (3.14)$$

$$p_{i3} = Tr(P_i\Lambda(\rho_3^{error})) = (p[Tr(P_i\Lambda(|x\rangle\langle x|))] + (1-p)[Tr(P_i\Lambda(\delta_3))]) \quad (3.15)$$

$$p_{i4} = Tr(P_i\Lambda(\rho_4^{error})) = (p[Tr(P_i\Lambda(|y\rangle\langle y|))] + (1-p)[Tr(P_i\Lambda(\delta_4))]) \quad (3.16)$$

Measurement Error

For the measurement Errors:

$$p_{i1} = Tr(P_i^{Error}\Lambda(\rho_1)) = (p[Tr(P_i\Lambda(|0\rangle\langle 0|))] + (1-p)[Tr(\kappa_i\Lambda(\rho_1))]) \quad (3.17)$$

$$p_{i2} = Tr(P_i^{Error}\Lambda(\rho_2)) = (p[Tr(P_i\Lambda(|1\rangle\langle 1|))] + (1-p)[Tr(\kappa_i\Lambda(|1\rangle\langle 1|))]) \quad (3.18)$$

$$p_{i3} = Tr(P_i^{Error}\Lambda(\rho_3)) = (p[Tr(P_i\Lambda(|x\rangle\langle x|))] + (1-p)[Tr(\kappa_i\Lambda(|x\rangle\langle x|))]) \quad (3.19)$$

$$p_{i4} = Tr(P_i^{Error}\Lambda(\rho_4)) = (p[Tr(P_i\Lambda(|y\rangle\langle y|))] + (1-p)[Tr(\kappa_i\Lambda(|y\rangle\langle y|))]) \quad (3.20)$$

Initialization and Measurement Error

And for both the initialization and measurement Errors:

$$p_{i1} = Tr(P_i^{error}\Lambda(\rho_1^{error})) = Tr[(p^{meas}P_i + (1-p^{meas})\kappa_i)\Lambda(p^{init}(|0\rangle\langle 0| + (1-p^{init})\delta_1)] \quad (3.21)$$

$$p_{i2} = Tr(P_i^{error}\Lambda(\rho_2^{error})) = Tr[(p^{meas}P_i + (1-p^{meas})\kappa_i)\Lambda(p^{init}(|1\rangle\langle 1| + (1-p^{init})\delta_2)] \quad (3.22)$$

$$p_{i3} = Tr(P_i^{error}\Lambda(\rho_3^{error})) = Tr[(p^{meas}P_i + (1-p^{meas})\kappa_i)\Lambda(p^{init}(|x\rangle\langle x| + (1-p^{init})\delta_3)] \quad (3.23)$$

$$p_{i4} = Tr(P_i^{error}\Lambda(\rho_4^{error})) =$$
$$Tr[(p^{meas}P_i + (1-p_0^{meas})\kappa_i)\Lambda(p^{init}(|y\rangle\langle y| + (1-p^{init})\delta_4)] \tag{3.24}$$

A final note on the general form for our errors: we will refer to "scattered" when we consider that the probability of complete success in one measurement or initialization state "p" might differ for other initialization or measurement. This means that different p_{ij} could have different probabilities p inside them. Here we have written them all as "p" to simplify the notation. This applies to the 2 qubit case as well.

3.2 Two qubit implementation

Theoretically, we can expand this method further to more qubits easily. For two qubits, we show the general form p_{ij} and A_{ijpq} takes.

We note that for this case $p_{ij}, i \in \{1, 16\}$ and $j \in \{1, 16\}$ which corresponds to the number of probabilities measurements we require. In total, 256 measurements are required

Again, we flatten p_{ij} as p_α. Which makes it a 256x1 matrix.

For the case of A_{ijpq} it is a 256x256 matrix . It therefore counts with 65,536 elements. This is computationally heavy. Specially since we have to calculate its inverse. However, as previously mentioned, we recycle this value for all gates in the two qubit case.

Similarly, as before, we obtain $\chi_{pq} = A^{-1}_{ijpq}.p_{pq}$. We then use this value to reconstruct the gates by performing the following summation:

$$\Lambda_1 \otimes \Lambda_2(\varrho)\Lambda_2^\dagger \otimes \Lambda_1^\dagger = \sum_{ij} \chi_{ij}(\sigma\otimes\sigma)_i \varrho (\sigma\otimes\sigma)_j^\dagger \tag{3.25}$$

We take the following set of as our complete set of operators: $\sigma_i \otimes \sigma_j =$

$$\begin{aligned}\{&Id\otimes Id, Id\otimes X, Id\otimes Y, Id\otimes Z, X\otimes Id, X\otimes X, X\otimes Y, X\otimes Z,\\ &Y\otimes Id, Y\otimes X, Y\otimes Y, Y\otimes Z, Z\otimes Id, Z\otimes X, Z\otimes Y, Z\otimes Z\}\end{aligned} \tag{3.26}$$

Then for our initialization and projector states, we take the complete set:

$$\varrho_1 = P_1 = |0\rangle\langle 0| \otimes |0\rangle\langle 0| \tag{3.27}$$

$$\varrho_2 = P_2 = |0\rangle\langle 0| \otimes |1\rangle\langle 1| \tag{3.28}$$

$$\varrho_3 = P_3 = |0\rangle\langle 0| \otimes |x\rangle\langle x| \tag{3.29}$$
$$\varrho_4 = P_4 = |0\rangle\langle 0| \otimes |y\rangle\langle y| \tag{3.30}$$
$$\varrho_5 = P_5 = |1\rangle\langle 1| \otimes |0\rangle\langle 0| \tag{3.31}$$
$$\varrho_6 = P_6 = |1\rangle\langle 1| \otimes |1\rangle\langle 1| \tag{3.32}$$
$$\varrho_7 = P_7 = |1\rangle\langle 1| \otimes |x\rangle\langle x| \tag{3.33}$$
$$\varrho_8 = P_8 = |1\rangle\langle 1| \otimes |y\rangle\langle y| \tag{3.34}$$
$$\varrho_9 = P_9 = |x\rangle\langle x| \otimes |0\rangle\langle 0| \tag{3.35}$$
$$\varrho_{10} = P_{10} = |x\rangle\langle x| \otimes |1\rangle\langle 1| \tag{3.36}$$
$$\varrho_{11} = P_{11} = |x\rangle\langle x| \otimes |x\rangle\langle x| \tag{3.37}$$
$$\varrho_{12} = P_{12} = |x\rangle\langle x| \otimes |y\rangle\langle y| \tag{3.38}$$
$$\varrho_{13} = P_{13} = |y\rangle\langle y| \otimes |0\rangle\langle 0| \tag{3.39}$$
$$\varrho_{14} = P_{14} = |y\rangle\langle y| \otimes |1\rangle\langle 1| \tag{3.40}$$
$$\varrho_{15} = P_{15} = |y\rangle\langle y| \otimes |x\rangle\langle x| \tag{3.41}$$
$$\varrho_{16} = P_{16} = |y\rangle\langle y| \otimes |y\rangle\langle y| \tag{3.42}$$

General form of errors for two qubits SQPT

We see the most general form that errors we consider take:

Initialization Error

For the initialization error can view it as:

$$p_{i1} = Tr(P_i\Lambda(\rho_1^{error})) = (p[Tr(P_i\Lambda(|0\rangle\langle 0| \otimes |0\rangle\langle 0|))] + (1-p)[Tr(P_i\Lambda(\delta_1))]) \tag{3.43}$$

...

$$p_{i16} = Tr(P_i\Lambda(\rho_{16}^{error})) = (p[Tr(P_i\Lambda(|y\rangle\langle y| \otimes |y\rangle\langle y|))] + (1-p)[Tr(P_i\Lambda(\delta_{16}))]) \tag{3.44}$$

Measurement Error

For the measurement errors:

$$p_{i1} = Tr(P_i^{error}\Lambda(\rho_1)) = (p[Tr(P_i\Lambda(\rho_1))] + (1-p)[Tr(\kappa_i\Lambda(\rho_1))]) \quad (3.45)$$

...

$$p_{i16} = Tr(P_i^{error}\Lambda(\rho_{16})) = (p[Tr(P_i\Lambda(\rho_{16}))] + (1-p)[Tr(\kappa_i\Lambda(\rho_{16}))]) \quad (3.46)$$

Initialization and Measurement Error

And for both the initialization and measurement errors:

$$p_{i1} = Tr(P_i^{error}\Lambda(\rho_1^{error})) = Tr((p^{meas}P_i + (1-p^{meas})\kappa_i)\Lambda(p^{init}(|0\rangle\langle 0| \otimes |0\rangle\langle 0|) + (1-p^{init})\delta_1)) \quad (3.47)$$

...

$$p_{i16} = Tr(P_i^{error}\Lambda(\rho_{16}^{error})) = Tr((p^{meas}P_i + (1-p^{meas})\kappa_i)\Lambda(p^{init}(|y\rangle\langle y| \otimes |y\rangle\langle y|) + (1-p^{init})\delta_{16})) \quad (3.48)$$

3.3 Error modelling

In chapter 2, we gave a description between coherent and incoherent noise. In this section, we will continue our discussion about noise and we will describe and reason the ways we will model errors in initialisation and measurement. We will first provide the basics about possible representation and assumptions in our errors. We then move to deal with two key decisions in our work, choosing quantum vs classical noise and deciding which errors to model.

Assumptions in our method:

1 We have access to the statistics given by Born's rule. This is the so-called "frequentist approach to probability", which says that only if we repeated the experiment infinitely times, we would get the exact probability. We assume that this assumption is satisfied for a sufficient number of experiments. This is an assumption that we use when calculating the effect of these errors in SQPT, i.e. we are assuming the probability measurements we obtain reflect perfectly the effect of the noise.

2 It is a well-known fact that any quantum channel that corresponds to a physical process can be seen as a CPTP map. We therefore only consider CPTP maps. This is also key in SQPT since we can therefore write gates in terms of Kraus operators, as we showed.

3 We only consider incoherent errors and act on each qubits individually in the same way.

4 We only consider "classical" errors

Note that we do not consider coherent noise for input and measurement errors since the biggest focus on recent research is on incoherent errors. This also leads us to consider errors acting individually in qubits. And, as we clarify next, we only consider "classical" noise.

3.3.1 Single-qubit vs qubit-qubit interactions

We can consider single-qubit or qubit-qubit interactions.

Single-qubits errors: We refer to single qubit errors as those processes that affect each qubit individually, they are the ones that are sourced externally, such as, from the interaction with external fields. We can see these errors as a map $\mathcal{V}$ on the individual qubits:

$$\mathcal{V} \otimes \mathcal{V} \otimes \cdots \otimes \mathcal{V}$$

where each $\mathcal{V}$ is a single-qubit error operator.

Qubit-qubits errors: We consider this for the case of coherent errors, when interactions occur between data and ancilla qubits to modify the dynamics of the system. Note that these ancilla qubits can be syndrome qubits, i.e. used for error syndrome measurements. In fact, recent discoveries claim this could an important error happening in QEC [31]

In our work, as we mentioned, we will only look into single-qubit errors, as we are only modelling incoherent noise. The general form of initialization and measurement of these errors will be as follows:

$$\kappa_1 = \delta_1 = p_1 \Lambda_{Error_1} |0\rangle \langle 0| \Lambda^\dagger_{Error_1} \tag{3.49}$$

$$\kappa_2 = \delta_2 = p_2 \Lambda_{Error_2} |1\rangle \langle 1| \Lambda^\dagger_{Error_2} \tag{3.50}$$

$$\kappa_3 = \delta_3 = p_3 \Lambda_{Error_3} |z\rangle \langle z| \Lambda^\dagger_{Error_3} \tag{3.51}$$

$$\kappa_4 = \delta_4 = p_4 \Lambda_{Error_4} |w\rangle \langle w| \Lambda^\dagger_{Error_4} \tag{3.52}$$

We can generalise this to two qubits as well.

Note that we have represented p_0 to be our probability of abscense of errors. Together with p_i, they form a distribution of probabilities, i.e. $p_0 + p_i = 1$ for $i = 1, 2, 3, 4$. When we implement our model, we write each κ and δ with independent probabilities and gates in order to give the most general form. We will also apply two probability models:

- The first one is $p_1 = p_2 = p_3 = p_4$ i.e. we assume that the probability of encountering the error is constant in the system.

- The other one is $p_1 \neq p_2 \neq p_3 \neq p_4$, which we refer as "scattered" i.e. we assume that the probability p of error varies in each measurement/initialization. We have previously mentioned this, but now we can see what it means for this description of our model.

Also, we have specified a different gate applied to each state, however, in most of our cases we use: $\Lambda_{Error_1} = \Lambda_{Error_2} = \Lambda_{Error_3} = \Lambda_{Error_4}$. Only in one of our cases, we will consider these to be different. The reason for this is to provide a more general perspective on the effect of errors.

3.3.2 Classical vs quantum error

An interesting discussion to reflect on is on the possible interpretations of classical and quantum errors.

Classical Error modelling: By classical errors, we refer to those perturbations with a classical limit. To explain this further, we give an example of how classical noise affect measurement.

Let us denote the ideal vector of probabilities that one would have obtained from an ideal scenario as $\mathbf{p}^{\text{ideal}}$. We consider a function Λ_{Error} to be the error map in our system. Then for an arbitrary quantum state ρ, the vector of probabilities $\mathbf{p}_{\text{exp}}$ obtained in an experiment on a noisy device is given by

$$\mathbf{p}_{\text{exp}} = \Lambda \mathbf{p}_{\text{ideal}} \tag{3.53}$$

This is valid due to Born's rule. Proof:
From

$$P_i = Tr(P_i \Lambda(\rho)) \tag{3.54}$$

For a POVM P we distinguish between the erroneous and the ideal via the map:

$$P_i^{\text{exp}} = \sum_j p(i \mid j) P_j^{\text{ideal}} \tag{3.55}$$

where $i \in \{1, .., n\}$ and $p(i \mid j)$ respects two properties: $p(i \mid j) \in [0, 1]$, $\sum_i p(i \mid j) = 1$. The latter condition is added to assure that P^{exp} is a proper POVM. The value of n corresponds to number of quantum measurements performed. P^{exp} refers to erroneous POVM and P^{ideal} corresponds to the ideal POVM.

We can assume a similar idea of classical noise for the initialization states.

Quantum Error modelling:
We model these as deviations of some unitary rotation part. We take the generic notation adding the extra factor corresponding to quantum behaviour: $P^{exp} = \Lambda P^{ideal} + \triangle$ or $\rho^{exp} = \Lambda \rho^{ideal} + \triangle$ this would introduce an error: $p^{exp} = \Lambda p^{ideal} + \triangle^{'}$

Note that the method suggested in [53] to reduce this error leads to an optimisation problem, which should minimise the upper bound on the error of the error-mitigation procedure. We see it more clearly below by looking at the measure of the distance between classical probability distributions. This is the total-Variation (TV) distance:

$$D_{TV}\left(\Lambda^{-1}\mathbf{p}_{\text{exp}}, \mathbf{p}_{\text{ideal}}\right) = \frac{1}{2}\left\|\Lambda^{-1}\mathbf{p}_{\text{exp}} - \mathbf{p}_{\text{ideal}}\right\|$$

which we wish to minimise.

Due to the arbitrary decomposition one might make when segregating "classical" and "non-classical", we will not develop this further and we will leave this as a subjective discussion on how we can classify noise. In our study, we consider the case the non-classical part Δ is small compared to the term $\Lambda\mathbf{M}^{(\text{ideal})}$, and we neglect the "non classical" part. Taking this assumption, we therefore only consider "classical" noise in our technique.

3.3.3 Error models

We can represent error processes in a number of ways. The key points are that these will be changes in the phase and state. We see this in our models for incoherent noise. As specified, we are considering: incoherent "classical" single-qubit noise, modelled as CPTP maps. Another key point is that Initialization and measurements errors are modelled the same way for incoherent error models.

We will model several popular incoherent errors. The most common way to model these are in terms of the Kraus operators. For a general arbitrary error map of the density matrix, which satisfies all our conditions above, we consider a general Kraus map to model our error on a multi-qubit density matrix as follows

$$\rho \to \sum_k A_k^\dagger \rho A_k$$

where $\sum A_k^\dagger A_k = I$.

Non-Pauli channel noise

We first look at our application of an incoherent noise written in terms of a Non-Pauli matrix

The amplitude damping channel: This channel refers to the qubit falling from an excited state to a ground state through spontaneous emission.

The Kraus operator elements of the channel can be written as:

$$A_1 = \begin{pmatrix} 1 & 0 \\ 0 & \sqrt{1-\gamma} \end{pmatrix}, A_2 = \begin{pmatrix} 0 & \sqrt{\gamma} \\ 0 & 0 \end{pmatrix}$$

$$\boldsymbol{\rho} \mapsto \Lambda_{Error}(\boldsymbol{\rho}) = \boldsymbol{M}_0 \boldsymbol{\rho} \boldsymbol{M}_0^\dagger + \boldsymbol{M}_1 \boldsymbol{\rho} \boldsymbol{M}_1^\dagger$$

The form of the operator elements indicate that this channel is not a Pauli channel.

Pauli channel noise

On the other hand, we model Pauli channels. These are quantum channels that apply an n-qubit Pauli operator. They have been the most common way to model errors, especially for the models applied in Quantum Error Correction Codes. We can emphasize their relevance from the studies on the randomized compiling [54]. This is a technique which maps noise to a Pauli channel. This is very powerful because this has lead to very positive reductions of noise

We consider a general Pauli error as follows:

$$\rho \to (1 - p_x - p_y - p_z)\,\rho + p_x X \rho X + p_y Y \rho Y + p_z Z \rho Z$$

We discuss 2 examples of Pauli channels modelled as noise.

1. The depolarizing channel: This channel refers to a qubit getting to the completely mixed state $\rho = \frac{1}{2}I$ with probability p, and remaining intact with probability $1 - p$. The parameter p indicates the strength of depolarization, and it is the only parameter of this channel. The Kraus operator elements of the channel are the following:

$$A_1 = \sqrt{1 - \frac{3}{4}p}I, A_2 = \frac{1}{2}\sqrt{p}X, A_3 = \frac{1}{2}\sqrt{p}Y, A_4 = \frac{1}{2}\sqrt{p}Z$$

We see three types of depolarizing channels:

- **Bit-flip errors**: Initialization and measurements are usually bit flip (X). We implement the error as follows:

$$\Lambda_{Error} = \sqrt{p}X$$

- **Phase-flip errors**: We implement the error as follows:

$$\Lambda_{Error} = \sqrt{p}Z$$

- **Bit-flip and Phase-flip errors**: We implement the error as follows:

$$\Lambda_{Error} = \sqrt{p}Y$$

Note that because all the operator elements can be written as a Pauli matrix or identity multiplied with a scalar factor, this channel belongs to the more general class of Pauli channels. We note that we will only include Bit-Flip in our results graphs, due to the similarity in the effect of the three of them.

2. The phase damping channel: it represents the loss of quantum information. The Kraus operator elements of this channel are:

$$A_1 = \sqrt{p}I = \begin{pmatrix} \sqrt{p} & 0 \\ 0 & \sqrt{p} \end{pmatrix}, A_2 = \sqrt{1-p}Z = \begin{pmatrix} \sqrt{1-p} & 0 \\ 0 & -\sqrt{1-p} \end{pmatrix}$$

$\Lambda_{Error} = \sum_a \boldsymbol{M}_a \boldsymbol{\rho} \boldsymbol{M}_a = \left(1 - \frac{1}{2}p\right)\boldsymbol{\rho} + \frac{1}{2}p\boldsymbol{Z}\boldsymbol{\rho}\boldsymbol{Z}$

As can be seen from the form of the operator elements, this channel also is a Pauli channel.

Besides these maps, we model two simple "custom" errors. For simplicity, we define these in terms of their direct application, δ and κ:

The custom orthogonal error: To exploit the limits of errors, we encode errors for one qubit by considering an application of a unitary gate that turns the state into its orthogonal state. This means that for the base $\{|0\rangle, |1\rangle\}$ we will consider the error to turn $|0\rangle \rightarrow |1\rangle$ and vice versa. For the case of the $|x\rangle$ and $|y\rangle$ gates we find their orthogonal counterpart. An universal NOT gate does not exist, and it is for this reason that we model the error in the following way:

$$\kappa_1 = \delta_1 = p_1 |1\rangle \langle 1|$$
$$\kappa_2 = \delta_2 = p_2 |0\rangle \langle 0|$$
$$\kappa_3 = \delta_3 = p_3 |z\rangle \langle z|$$
$$\kappa_4 = \delta_4 = p_4 |w\rangle \langle w|$$

Note that taking the definition of f and g being orthogonal if their inner product (equivalently, the value of this integral) is zero: $\langle f, g\rangle = 0$, we discover the orthogonal states for $|x\rangle$ and $|y\rangle$ to be as follows:

- For $|x\rangle$ the orthogonal state is $|z\rangle = \frac{1}{\sqrt{2}}(|0\rangle - |1\rangle)$
- For $|y\rangle$ the orthogonal state is $|w\rangle = \frac{1}{\sqrt{2}}(|0\rangle - i\,|1\rangle)$

The custom rotation of states error: this second error we use it to investigate on the possible "rotations" of the states, we use:

$$\delta_1 = p_2\rho_2 + p_3\rho_3 + p_4\rho_4$$
$$\delta_2 = p_5\rho_1 + p_6\rho_3 + p_7\rho_4$$
$$\delta_3 = p_8\rho_1 + p_9\rho_2 + p_{10}\rho_4$$
$$\delta_4 = p_{11}\rho_1 + p_{12}\rho_2 + p_{13}\rho_3$$

and for the errors in the projectors:

$$\kappa_1 = p_2P_2 + p_3P_3 + p_4P_4$$
$$\kappa_2 = p_5P_1 + p_6P_3 + p_7P_4$$
$$\kappa_3 = p_8P_1 + p_9P_2 + p_{10}P_4$$
$$\kappa_4 = p_{11}P_1 + p_{12}P_2 + p_{13}P_3$$

Note that due to computational overhead, we only compute this for one qubit.

Specially, for the scattered case, this becomes complicated as each κ and δ have 4 different sets of probability distributions.

3.4 χ Fidelity Calculation

Following our implementation, we discuss our choice of formula to calculate the Fidelity and its calculation for one and two qubits.

To calculate fidelity, we make a choice of the following formula [55]

$$F = \frac{Tr((\chi)\chi^{\dagger}_{ideal})}{\sqrt{Tr((\chi_{ideal} + \chi_{faulty})^{\dagger}(\chi_{ideal} + \chi_{faulty}))}\sqrt{Tr(\chi^{\dagger}_{th}\chi_{th})}} \tag{3.56}$$

This decision alleviates computational costs as we can work directly with the χ matrices, instead of with the full reconstructed map, as we saw in section 2.4.

We also note that instead of plotting against fidelity. We plot in the log-log scale against infidelity.

Chapter 4

Results and beyond

In this chapter, we present and analyse the results of our selected models. We additionally explain further some implementation details on each that we did not mention before.

In our plots, we assumed that the probability of suffering input and measurement errors is rather low, hence we only look at the case where the presence of errors is between 0 and 10%, unless otherwise stated.

To evaluate the effect of these errors on the gate fidelity, we plot the "probability of no errors", against the "Infidelity". The probability of no errors ranges between 0 and 1. This is the probability of the absence of the error. The other term, "Infidelity", is 1 - Gate Fidelity.

We also plot in the Log scale to see more clearly how the fidelity behaves.

In our plots, we make use of 2 random sets of probabilities, the first set contains 100 distribution of probabilities, and the second one, 1000. We will specify when either one is used. The use of one larger set of points over the other is dependent on the computational cost of the gate reconstruction.

We also point out that the probability of no errors is calculated as (probability of no errors in the initialization + probability of no errors in the measurement)/2 when both errors are implemented. Also, note that in most cases, the input and measurement errors have the same distribution. Therefore one hides the other in the graph.

4.1 One qubit

To model the gate reconstruction, we have worked with the qubit gates X,Y,Z. However, we have seen a very similar effect on the three of them. Therefore we will just illustrate the assessment of fidelity for the X gate, except for the phase damping gate.

4.1.1 Orthogonal and Rotational Error

We use the random set of 1000 probability distributions for the orthogonal errors and 100 for the rotational errors, due to computational cost. We note that we use the two types of probability models for Measurement and Input Errors as we mentioned before.

We remind the reader that in the plots, we use the probability of the absence of error from 0 to 1. Also, our plots are in the log-log scale to illustrate the gate fidelity against the probability of no errors appearing.

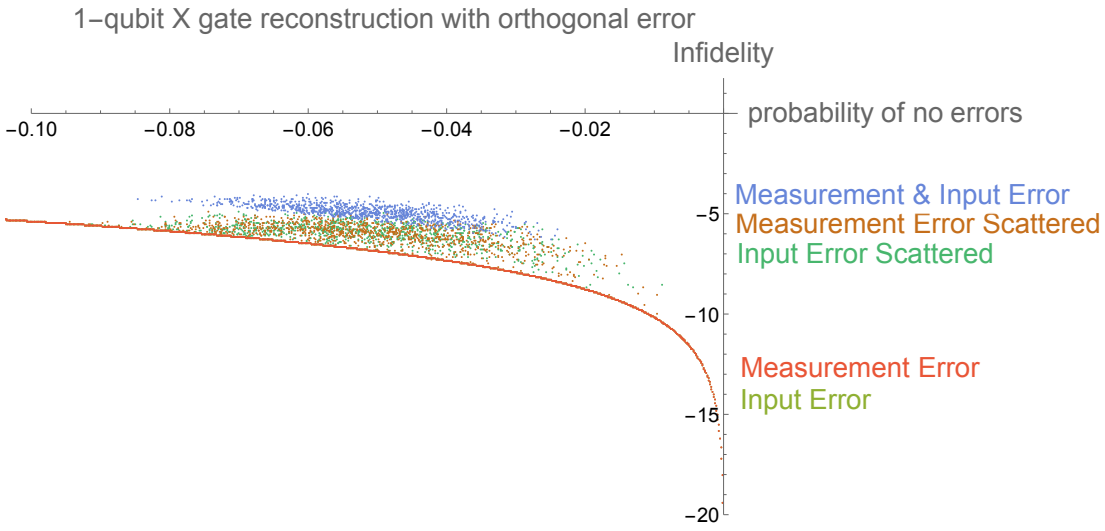

Figure 4.1: Custom orthogonal error affecting the 1-qubit X gate fidelity for input, measurement and both errors.

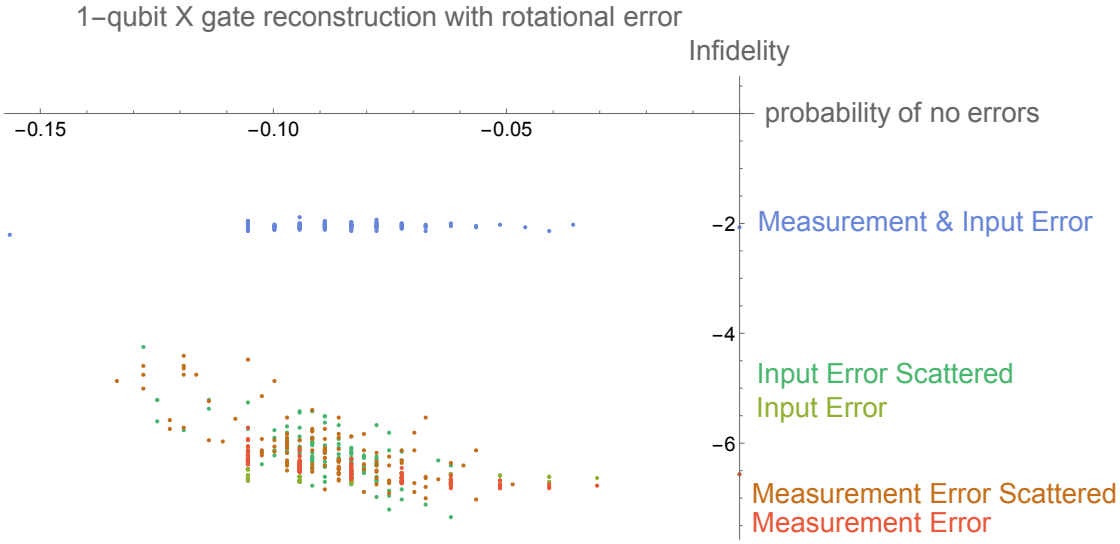

Figure 4.2: Custom rotational error affecting the 1-qubit X gate fidelity for input, measurement and both errors.

4.1.2 Amplitude Damping Error

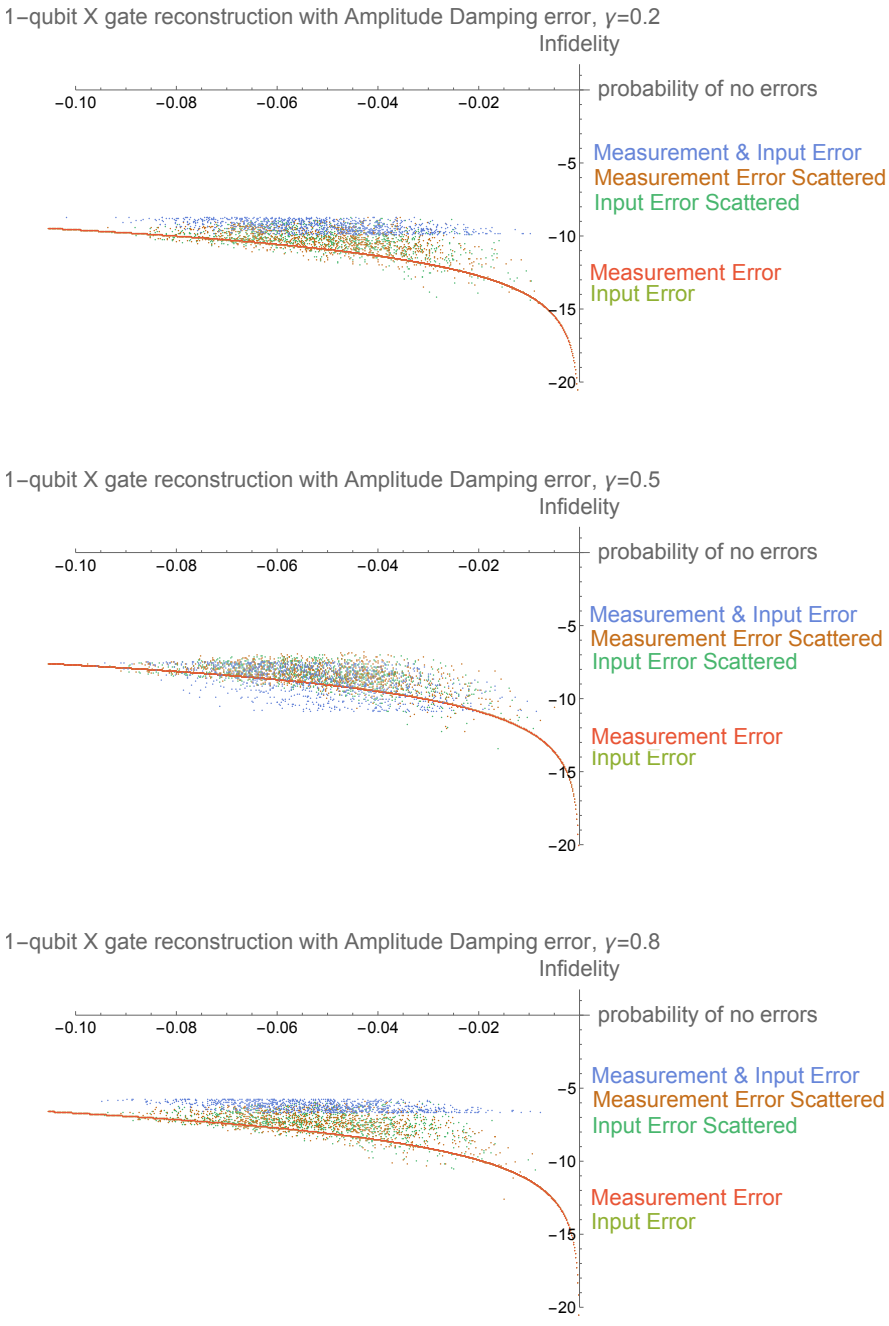

Figure 4.3: Amplitude damping error affecting the 1-qubit X gate fidelity for input, measurement and both errors. We show 3 plots for different γ values

4.1.3 Depolarizing Error

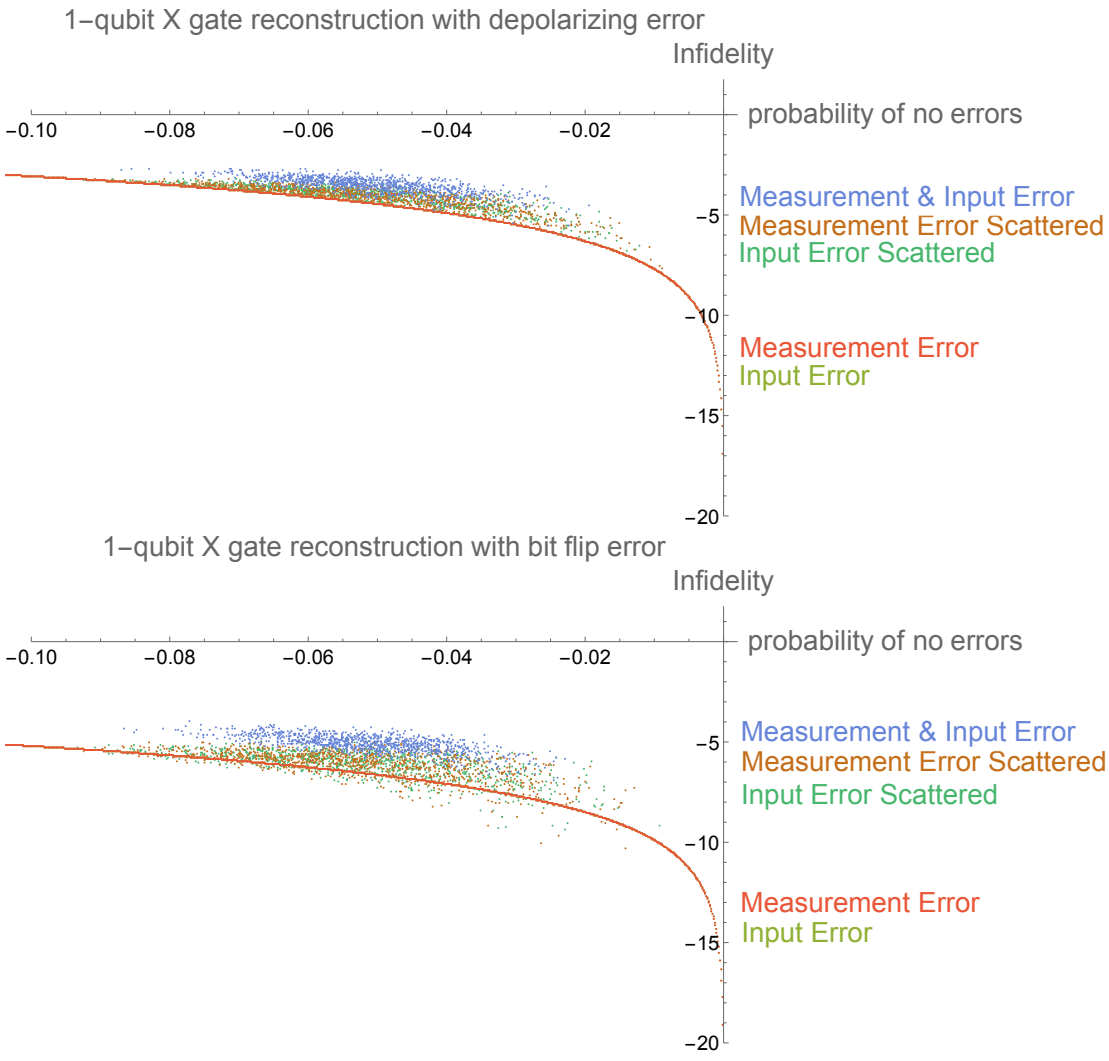

Figure 4.4: General Depolarizing and Bit flip error affecting the 1-qubit X gate fidelity for input, measurement and both errors.

4.1.4 Phase Damping Error

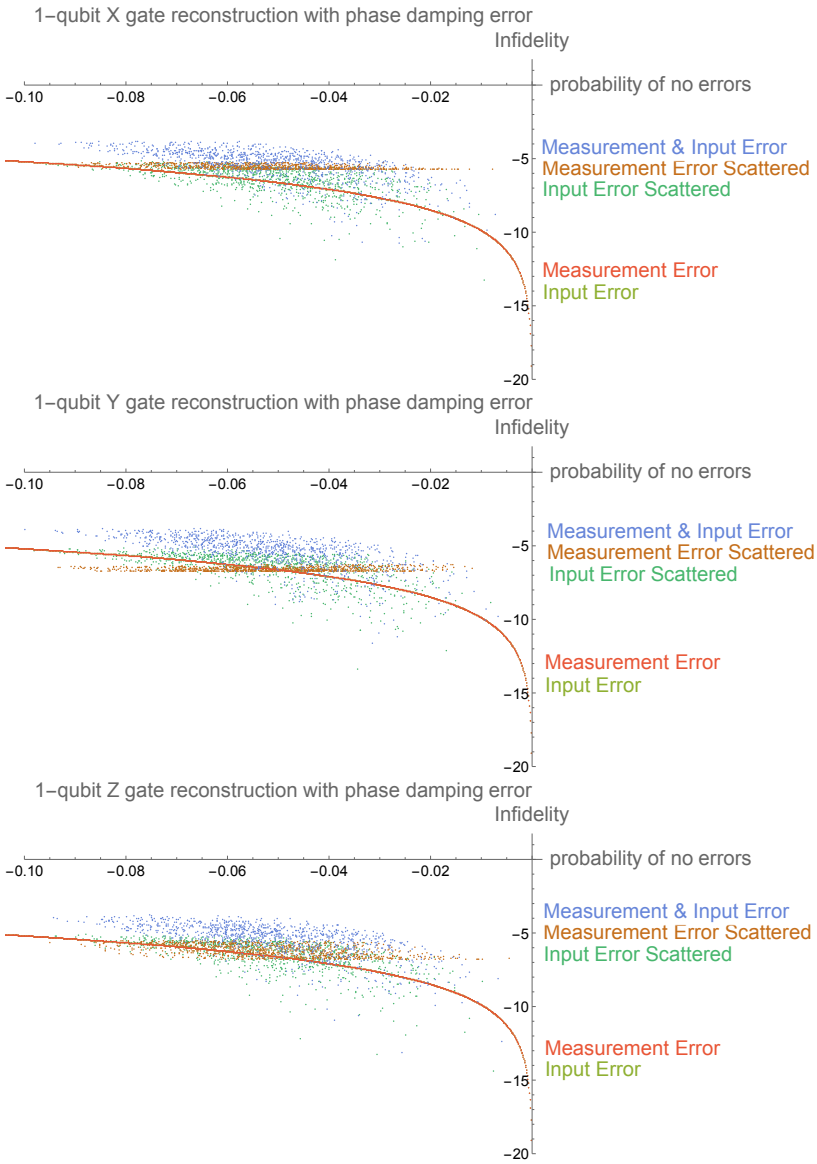

Figure 4.5: Phase damping error affecting the 1-qubit X,Y,Z gate fidelity for input, measurement and both errors.

In this case, we plot against the three Pauli gates, since we see a slight different effect on the quality of the dynamics. We believe that this could be due to the model used for the probabilities.

4.2 Two qubit

In a very similar fashion to the 1-qubit case, we now we look for the cases of 2 qubit gate Reconstruction. We apply the gates as we refered to single qubits operations. Also, We use a less big randomisation of the errors to reduce time cost in the calculations.

Note that here we do not compute the graph for our custom rotational error. This is not very important as the whole purpose of introducing such error was for us to see a more complete and diverse error modelling.

4.2.1 Orthogonal Error

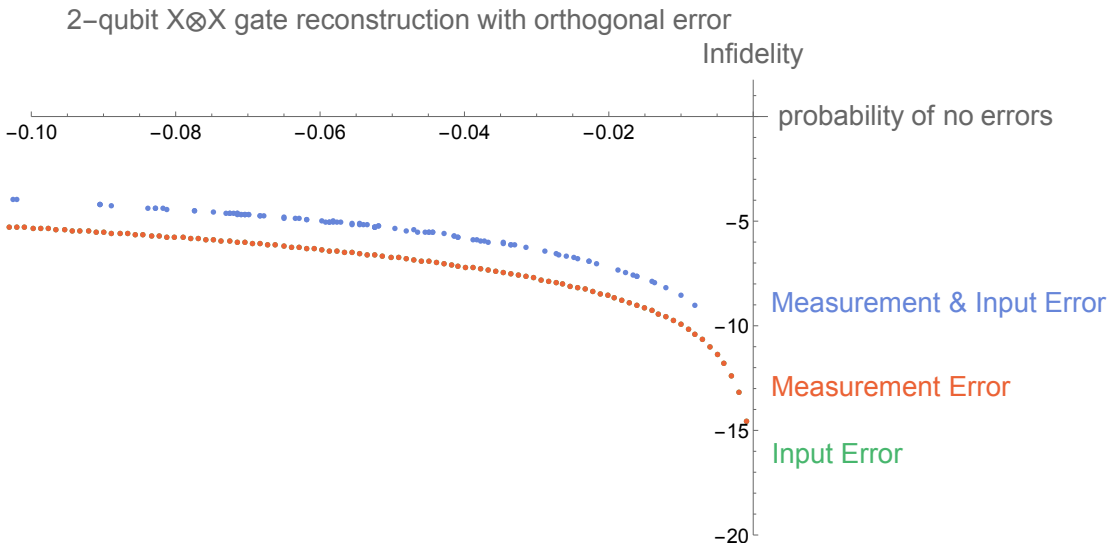

Figure 4.6: Custom orthogonal error affecting the 2-qubit XxX gate fidelity for input, measurement and both errors.

4.2.2 Amplitude Damping Error

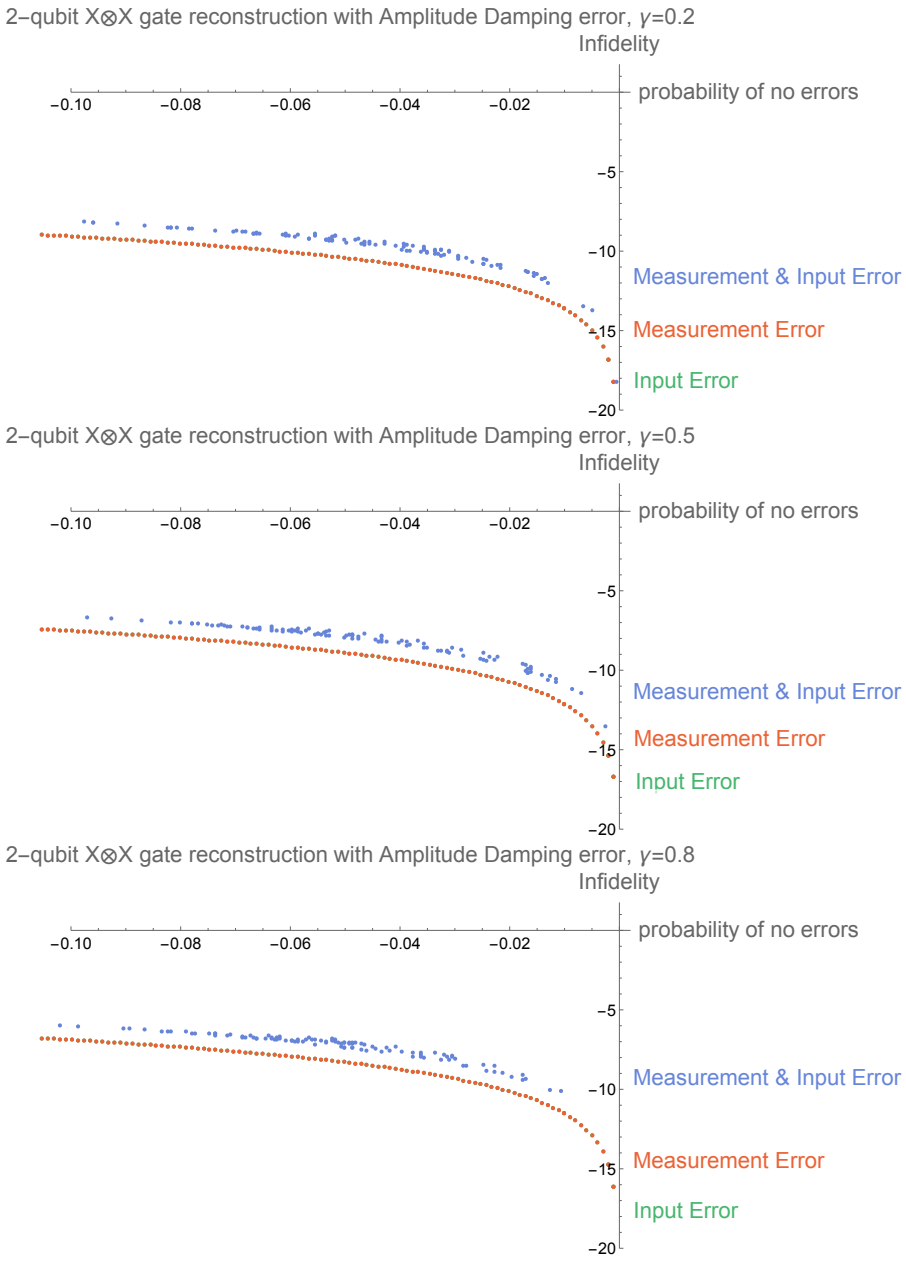

Figure 4.7: Amplitude damping error affecting the 2-qubit XxX gate fidelity for input, measurement and both errors. We show 3 plots for different γ values

4.2.3 Depolarizing Error

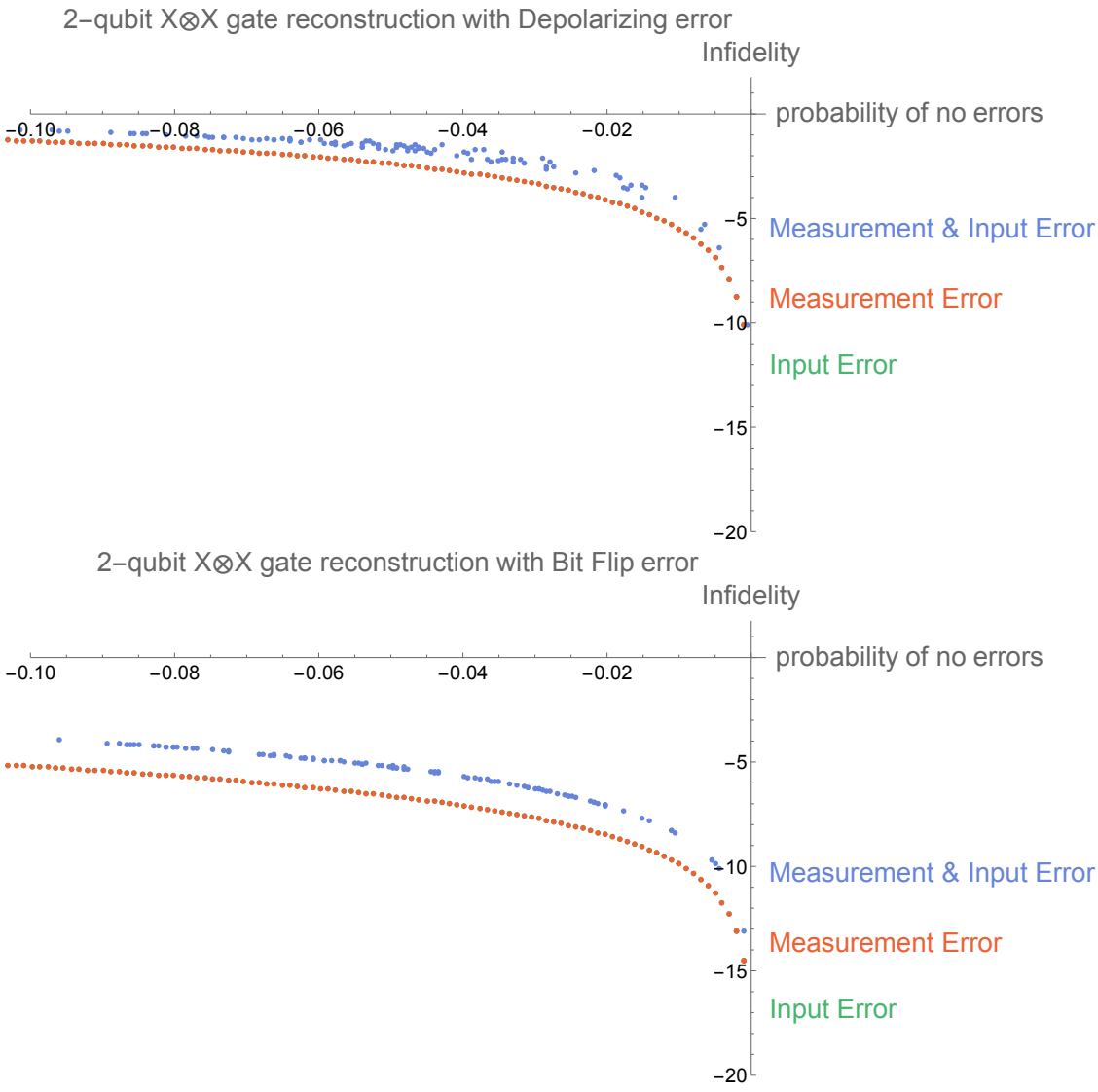

Figure 4.8: General depolarizing and Bit flip error affecting the 2-qubit XxX gate fidelity for input, measurement and both errors.

As we can see the general depolarizing error translates to a a bigger reduction in the quality of the dynamics.

4.2.4 Phase Damping Error

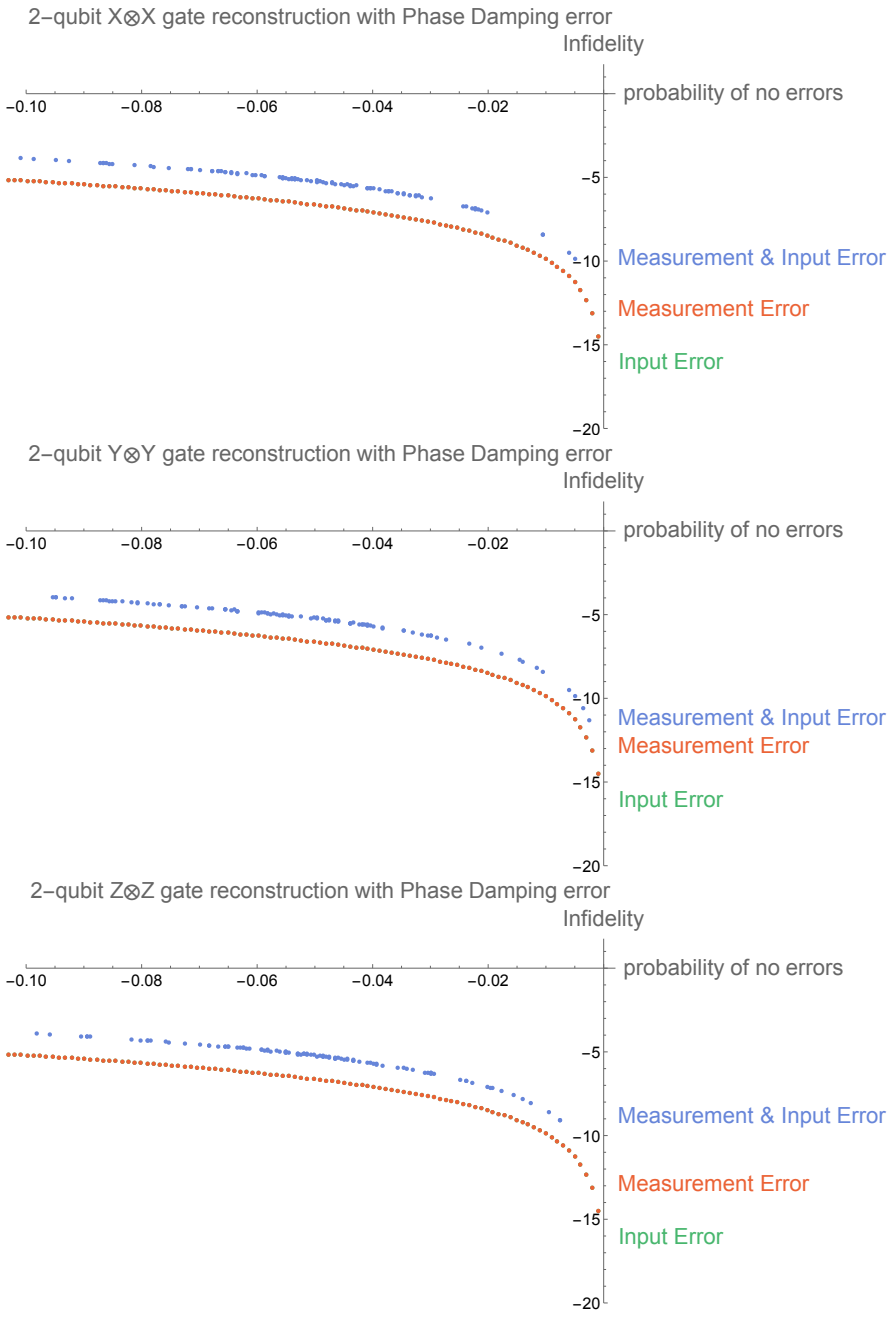

Figure 4.9: Phase damping error affecting the 2-qubit XxX, YxY, ZxZ gate fidelity for input, measurement and both errors.

4.3 Beyond our method

We classify the limitations to our method into two categories: computational and experimental.

4.3.1 Experimental limitations

We can think of some experimental limitations to be linked to the fact that SQPT has theoretical limitations. Linear inversion is a very clean method which relies on being able to calculate experimentally $\chi = A_{ijpq} p_{exp}$ to invert $\mathcal{E}(\rho) = \sum_{\alpha,\beta=1}^{d^2} \chi_{\alpha\beta} A_\alpha \rho A_\beta^\dagger$. We note that 2 of our assumptions was that the reconstructed map and the error map had to be CPTP which assures the process is physical. However, experimentally, the p_{exp} measured leads to a non hermitian matrix. In standard QPT this problem is remedied by minimizing (in some sense) the difference between the probabilities p_{ideal} and the experimental probabilities p_{exp}. [56]. This method is referred to as the **Least Squared method**, and it consists on minimizing the difference as $\min \sum_j \left[P_j^{\text{exp}} - P_j^{ideal}\right]^2$

Another technique commonly implemented to deal with these experimental issues is the Maximum Likelihood.

Maximum Likelihood

The trick to deal with these unphysical matrices is that the maximum-likelihood method leaves out the negative-eigenvalues (non-physical). The key of the method is to reconstruct the quantum state by $\rho = \arg\max_\rho \{\mathcal{C}(\rho, X)\}$ for the constraint $\rho \geq 0$ where $\mathcal{C}$ represents the likelihood of ρ generating the set X of observed data, i.e. undergoing the process we are looking for. It estimates P_j^{ideal} from the measurement data by finding values for the parameter that maximise the likelihood of having obtained the measurement outcomes.

Another type of challenges in the experiment in the number of states and measurements one must perform. QPT requires 2^{4N} measurements to be performed i.e. 12 measurements for one qubit in total. In fact, experimentally, Quantum Tomography has been performed only up to 3 qubits [57].

An important alternative for these experimentally heavy tomography methods, especially for the one and two qubit case, is the application of the

Choi-Jamiolkowski (CJ) isomorphism [58] [59]. This isomorphisms relates the QPT for N qubits to a QST of 2N qubits maximally entabled quantum states where N qubits have undergone through the process we are trying to reconstruct. This translates to a reduce in total measurements.

4.3.2 Computational limitations

We have performed our method for one and two qubits, beyond two qubits there are computational limitations to perform the QPT and the fidelity assessment we have discussed. One example is when we compute the matrix A_{ijpq}, which is of size: $d^{2^{2N}} \times d^{2^{2N}}$. This therefore means that calculating χ becomes too difficult to handle.

We can also see that computing the modelled errors described above also become very computationally challenging for large sets of probability distributions.
Therefore we can see that for a further number of qubits we require other techniques. One nice option are the current advances in machine learning applied to tomography, such as [60]

Chapter 5

Conclusions

We can conclude that, the classical incoherent errors in the initialization and measurement have a small effect on a quantum process. In the log-log scale, we can see that the effect of the error decays with an asymptotic behaviour as the probability of errors reduces to 0. This translates to a negligible effect on the fidelity if the probability of the presence of errors is minimal. We see that the fidelity decay depends on the classical error applied.
Overall, the effects of the quantum errors do not seem to have a big dependence on the system's dynamics, as we have found considerably similar distributions on the fidelity for different gate reconstructions.
We can see a similar effect on both the 1 qubit and the 2 qubits case. This is something we expected given the single qubit model we used. We can further deduce similar results for more qubits. Besides this, we see a comparable effect between input and measurement errors. As expected, we see a decrease in the dynamics quality once both are introduced.

To summarise, the outcome of this study is that an effective implementation of a quantum system is considerably independent of the erroneous applications in the measurement and input. This result is within the bounds of the CPTP maps representing incoherent noise that we chose and the assumptions that we made. Given the connection of general noise to this type of maps, we can also expect many other errors to have a similar effect.

Bibliography

[1] V. Silva, "Quantum computing: Bending the fabric of reality itself," in *Practical Quantum Computing for Developers*, pp. 23–76, Springer, 2018.

[2] G. Q. AI, "Exponential suppression of bit or phase errors with cyclic error correction," *Nature*, vol. 595, no. 7867, p. 383, 2021.

[3] J. Preskill, "Quantum computing in the nisq era and beyond," *Quantum*, vol. 2, p. 79, 2018.

[4] G. Li, Y. Ding, and Y. Xie, "Tackling the qubit mapping problem for nisq-era quantum devices," in *Proceedings of the Twenty-Fourth International Conference on Architectural Support for Programming Languages and Operating Systems*, pp. 1001–1014, 2019.

[5] K. Temme, S. Bravyi, and J. M. Gambetta, "Error mitigation for short-depth quantum circuits," *Physical review letters*, vol. 119, no. 18, p. 180509, 2017.

[6] S. Greenaway, F. Sauvage, K. E. Khosla, and F. Mintert, "Efficient assessment of process fidelity," *arXiv preprint arXiv:2102.08101*, 2021.

[7] A. B. Finnila, M. Gomez, C. Sebenik, C. Stenson, and J. D. Doll, "Quantum annealing: A new method for minimizing multidimensional functions," *Chemical physics letters*, vol. 219, no. 5-6, pp. 343–348, 1994.

[8] C. Neill, T. McCourt, X. Mi, Z. Jiang, M. Niu, W. Mruczkiewicz, I. Aleiner, F. Arute, K. Arya, J. Atalaya, *et al.*, "Accurately computing the electronic properties of a quantum ring," *Nature*, vol. 594, no. 7864, pp. 508–512, 2021.

[9] J. Zhang, G. Pagano, P. W. Hess, A. Kyprianidis, P. Becker, H. Kaplan, A. V. Gorshkov, Z.-X. Gong, and C. Monroe, "Observation of a many-body dynamical phase transition with a 53-qubit quantum simulator," *Nature*, vol. 551, no. 7682, pp. 601–604, 2017.

[10] F. Arute, K. Arya, R. Babbush, D. Bacon, J. C. Bardin, R. Barends, R. Biswas, S. Boixo, F. G. Brandao, D. A. Buell, *et al.*, "Quantum supremacy using a programmable superconducting processor," *Nature*, vol. 574, no. 7779, pp. 505–510, 2019.

[11] H.-S. Zhong, H. Wang, Y.-H. Deng, M.-C. Chen, L.-C. Peng, Y.-H. Luo, J. Qin, D. Wu, X. Ding, Y. Hu, *et al.*, "Quantum computational advantage using photons," *Science*, vol. 370, no. 6523, pp. 1460–1463, 2020.

[12] P. W. Shor, "Algorithms for quantum computation: discrete logarithms and factoring," in *Proceedings 35th annual symposium on foundations of computer science*, pp. 124–134, Ieee, 1994.

[13] A. K. Lenstra, H. W. Lenstra, M. S. Manasse, and J. M. Pollard, "The number field sieve," in *The development of the number field sieve*, pp. 11–42, Springer, 1993.

[14] J. Preskill, "Quantum computing and the entanglement frontier," *arXiv preprint arXiv:1203.5813*, 2012.

[15] Y. Wu, W.-S. Bao, S. Cao, F. Chen, M.-C. Chen, X. Chen, T.-H. Chung, H. Deng, Y. Du, D. Fan, *et al.*, "Strong quantum computational advantage using a superconducting quantum processor," *arXiv preprint arXiv:2106.14734*, 2021.

[16] I. Kerenidis and A. Prakash, "Quantum recommendation systems," *arXiv preprint arXiv:1603.08675*, 2016.

[17] M. Cerezo, A. Arrasmith, R. Babbush, S. C. Benjamin, S. Endo, K. Fujii, J. R. McClean, K. Mitarai, X. Yuan, L. Cincio, *et al.*, "Variational quantum algorithms," *Nature Reviews Physics*, pp. 1–20, 2021.

[18] P. Kaye, R. Laflamme, M. Mosca, *et al.*, *An introduction to quantum computing*. Oxford University Press on Demand, 2007.

[19] V. Armaos, D. A. Badounas, P. Deligiannis, and K. Lianos, "Computational chemistry on quantum computers," *Applied Physics A*, vol. 126, no. 8, pp. 1–7, 2020.

[20] Y. Suzuki, H. Yano, R. Raymond, and N. Yamamoto, "Normalized gradient descent for variational quantum algorithms," *arXiv preprint arXiv:2106.10981*, 2021.

[21] S. S. Tannu and M. K. Qureshi, "Mitigating measurement errors in quantum computers by exploiting state-dependent bias," in *Proceedings of the 52nd Annual IEEE/ACM International Symposium on Microarchitecture*, pp. 279–290, 2019.

[22] C. Ryan-Anderson, J. Bohnet, K. Lee, D. Gresh, A. Hankin, J. Gaebler, D. Francois, A. Chernoguzov, D. Lucchetti, N. Brown, *et al.*, "Realization of real-time fault-tolerant quantum error correction," *arXiv preprint arXiv:2107.07505*, 2021.

[23] J. Tuorila, M. Partanen, T. Ala-Nissila, and M. Möttönen, "Efficient protocol for qubit initialization with a tunable environment," *npj Quantum Information*, vol. 3, no. 1, pp. 1–12, 2017.

[24] T. Noh, G. Park, S.-G. Lee, W. Song, and Y. Chong, "Construction of controlled-not gate based on microwave-activated phase (map) gate in two transmon system," *Scientific reports*, vol. 8, no. 1, pp. 1–9, 2018.

[25] S. Sajeed, A. Ahmed, S. M. Ullah, and Z. H. Mozumder, "An approach to realize a quantum hadamard gate through optical implementation," in *2010 IEEE International Conference on Electro/Information Technology*, pp. 1–5, 2010.

[26] X.-M. Lin, Z.-W. Zhou, M.-Y. Ye, Y.-F. Xiao, and G.-C. Guo, "One-step implementation of a multiqubit controlled-phase-flip gate," *Physical Review A*, vol. 73, no. 1, p. 012323, 2006.

[27] M. Howard and J. Vala, "Qudit versions of the qubit $\pi/8$ gate," *Physical Review A*, vol. 86, no. 2, p. 022316, 2012.

[28] A. Kandala, K. Temme, A. D. Córcoles, A. Mezzacapo, J. M. Chow, and J. M. Gambetta, "Error mitigation extends the computational reach of a noisy quantum processor," *Nature*, vol. 567, no. 7749, pp. 491–495, 2019.

[29] M. H. Devoret and R. J. Schoelkopf, "Superconducting circuits for quantum information: an outlook," *Science*, vol. 339, no. 6124, pp. 1169–1174, 2013.

[30] S. Tannu and M. Qureshi, "Not all qubits are created equal," *arXiv preprint arXiv:1805.10224*, 2018.

[31] D. Greenbaum and Z. Dutton, "Coherent errors in quantum error correction," in *APS March Meeting Abstracts*, vol. 2017, pp. R51–007, 2017.

[32] A. Greene, M. Kjaergaard, M. Schwartz, G. Samach, A. Bengtsson, M. O'Keeffe, D. Kim, M. Marvian, A. Melville, B. Niedzielski, *et al.*, "Error mitigation via stabilizer measurement emulation," *arXiv preprint arXiv:2102.05767*, 2021.

[33] D. Gottesman, "An introduction to quantum error correction," in *Proceedings of Symposia in Applied Mathematics*, vol. 58, pp. 221–236, 2002.

[34] S. J. Beale, J. J. Wallman, M. Gutiérrez, K. R. Brown, and R. Laflamme, "Coherence in quantum error-correcting codes," *arXiv preprint arXiv:1805.08802*, 2018.

[35] P. W. Shor, "Scheme for reducing decoherence in quantum computer memory," *Physical review A*, vol. 52, no. 4, p. R2493, 1995.

[36] L. Egan, D. M. Debroy, C. Noel, A. Risinger, D. Zhu, D. Biswas, M. Newman, M. Li, K. R. Brown, M. Cetina, *et al.*, "Fault-tolerant control of an error-corrected qubit," *Nature*, pp. 1–6, 2021.

[37] B. Foxen, C. Neill, A. Dunsworth, P. Roushan, B. Chiaro, A. Megrant, J. Kelly, Z. Chen, K. Satzinger, R. Barends, *et al.*, "Demonstrating a continuous set of two-qubit gates for near-term quantum algorithms," *Physical Review Letters*, vol. 125, no. 12, p. 120504, 2020.

[38] P. Jurcevic, A. Javadi-Abhari, L. S. Bishop, I. Lauer, D. F. Bogorin, M. Brink, L. Capelluto, O. Günlük, T. Itoko, N. Kanazawa, *et al.*, "Demonstration of quantum volume 64 on a superconducting quantum computing system," *Quantum Science and Technology*, vol. 6, no. 2, p. 025020, 2021.

[39] M. Rol, F. Battistel, F. Malinowski, C. Bultink, B. Tarasinski, R. Vollmer, N. Haider, N. Muthusubramanian, A. Bruno, B. Terhal, *et al.*, "Fast, high-fidelity conditional-phase gate exploiting leakage interference in weakly anharmonic superconducting qubits," *Physical review letters*, vol. 123, no. 12, p. 120502, 2019.

[40] W. Huang, C. Yang, K. Chan, T. Tanttu, B. Hensen, R. Leon, M. Fogarty, J. Hwang, F. Hudson, K. M. Itoh, *et al.*, "Fidelity benchmarks for two-qubit gates in silicon," *Nature*, vol. 569, no. 7757, pp. 532–536, 2019.

[41] G. G. La Guardia, *Quantum Error Correction*. Springer, 2020.

[42] J. R. McClean, J. Romero, R. Babbush, and A. Aspuru-Guzik, "The theory of variational hybrid quantum-classical algorithms," *New Journal of Physics*, vol. 18, no. 2, p. 023023, 2016.

[43] S. Endo, Z. Cai, S. C. Benjamin, and X. Yuan, "Hybrid quantum-classical algorithms and quantum error mitigation," *Journal of the Physical Society of Japan*, vol. 90, no. 3, p. 032001, 2021.

[44] Y. Suzuki, S. Endo, K. Fujii, and Y. Tokunaga, "Quantum error mitigation for fault-tolerant quantum computing," *arXiv preprint arXiv:2010.03887*, 2020.

[45] D. F. James, P. G. Kwiat, W. J. Munro, and A. G. White, "On the measurement of qubits," in *Asymptotic Theory of Quantum Statistical Inference: Selected Papers*, pp. 509–538, World Scientific, 2005.

[46] R. Computing, "State tomography." https://forest-benchmarking.readthedocs.io/en/latest/examples/tomography$_s$*tate.html*.

[47] I. L. Chuang and M. A. Nielsen, "Prescription for experimental determination of the dynamics of a quantum black box," *Journal of Modern Optics*, vol. 44, no. 11-12, pp. 2455–2467, 1997.

[48] J. B. Altepeter, D. Branning, E. Jeffrey, T. Wei, P. G. Kwiat, R. T. Thew, J. L. O'Brien, M. A. Nielsen, and A. G. White, "Ancilla-assisted quantum process tomography," *Physical Review Letters*, vol. 90, no. 19, p. 193601, 2003.

[49] M. Mohseni and D. A. Lidar, "Direct characterization of quantum dynamics," *Physical Review Letters*, vol. 97, Oct 2006.

[50] C. Y. Li, *Adaptive Tomography of Pure States and Unitary Gates*. PhD thesis, 2017.

[51] M. A. Nielsen, "A simple formula for the average gate fidelity of a quantum dynamical operation," *Physics Letters A*, vol. 303, no. 4, pp. 249–252, 2002.

[52] J. Wang, Z.-Y. Han, S.-B. Wang, Z. Li, L.-Z. Mu, H. Fan, and L. Wang, "Scalable quantum tomography with fidelity estimation," *Physical Review A*, vol. 101, no. 3, p. 032321, 2020.

[53] F. B. Maciejewski, Z. Zimborás, and M. Oszmaniec, "Mitigation of readout noise in near-term quantum devices by classical post-processing based on detector tomography," *Quantum*, vol. 4, p. 257, 2020.

[54] J. J. Wallman and J. Emerson, "Noise tailoring for scalable quantum computation via randomized compiling," *Physical Review A*, vol. 94, no. 5, p. 052325, 2016.

[55] M. A. Nielsen and I. L. Chuang, "Quantum computation and quantum information," *Phys. Today*, vol. 54, no. 2, p. 60, 2001.

[56] A. V. Rodionov, A. Veitia, R. Barends, J. Kelly, D. Sank, J. Wenner, J. M. Martinis, R. L. Kosut, and A. N. Korotkov, "Compressed sensing quantum process tomography for superconducting quantum gates," *Physical Review B*, vol. 90, no. 14, p. 144504, 2014.

[57] T. Monz, "Quantum information processing beyond ten ion-qubits," 2011.

[58] A. Jamiołkowski, "Linear transformations which preserve trace and positive semidefiniteness of operators," *Reports on Mathematical Physics*, vol. 3, no. 4, pp. 275–278, 1972.

[59] M.-D. Choi, "Completely positive linear maps on complex matrices," *Linear algebra and its applications*, vol. 10, no. 3, pp. 285–290, 1975.

[60] G. Torlai, C. J. Wood, A. Acharya, G. Carleo, J. Carrasquilla, and L. Aolita, "Quantum process tomography with unsupervised learning and tensor networks," *arXiv preprint arXiv:2006.02424*, 2020.